Information and Computing Sciences
Faculty of Science, Utrecht University

Literature Review MSc Project — 2013

Master programme Game and Media Technology

A Literature Review for the Master Project: *Real-Time Musculoskeletal Model for Injury Simulation on 3D Human Characters*

ing. Francis P. Laclé

3503534

Supervisor: dr. N. Pronost

Contents

1 Introduction

Real-time musculoskeletal injuries for 3D human characters could be considered a next step in interactive media. It creates a possibility to alter a motion sequence depending on the type of injury that has been inflicted. This adds one extra layer of realism to the behaviour of the virtual human with respect to interactions with its virtual environment.

The simulation of musculoskeletal injuries in real-time can be of interest to serious applications such as surgical planning and training simulators, general medical training, forensics, evaluation of safety measures etc. In addition, less serious applications such as interactive storytelling in video games, where realism of animated human characters play an important role would also benefit from this extra layer of dynamic interaction. Real-time graphics and physics engines such as DICE's Frostbite 2 [6], Crytek's CryENGINE 3 [8], and Unreal Engine 3 [12] all strive for a visual and realistic representation of characters in their engines.

Modelling and simulating musculoskeletal injuries encompasses a multidisciplinary approach that goes beyond computational geometry and computer graphics taking other scientific fields such as anatomy and anthropometry, biomechanics and physiology, and structural analysis into consideration. Therefore, inclusion of literature that lies outside the scope of general computer graphics and animation is incorporated into this review. With respect to the musculoskeletal injuries themselves, literature is presented on several types such as fractures, tissue disruption, dislocations, sprains, strains, and amputations.

When it comes to simulating accurate wound physics, performance is still a challenge for current real-time engines due to the computational overhead involved with, among other things, non-linear dynamics. Due to this real-time constraint, the tradeoff between accuracy and performance is also discussed in section 3.1 of this review.

This review is organised as follows. The first two sections in the next chapter presents general scientific knowledge on topics that are uncommon in computer graphics and animation. The remaining two sections focus on the core of the topic, reviewing literature on soft tissue deformation, modelling of the musculoskeletal system, as well as a classification on types of musculoskeletal injuries coupled with contributions from respective fields. The final chapter discusses the master project, emphasising the implementation aspect as well as the role of accuracy versus performance, and ends with some concluding remarks.

2 The Literature Review

Studying musculoskeletal injuries of virtual humans covers a broad range of disciplines that includes, but not limited to, the science of human anatomy, anthropometry, and biomechanics. These will be discussed in the following subsections.

2.1 Human Anatomy

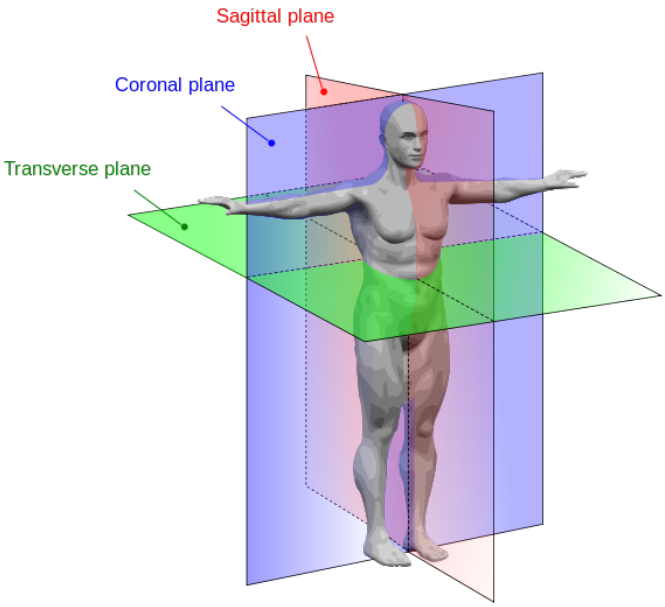

Figure 1: Human anatomy planes. The coronal plane divides the human body by length, the sagittal plane divides the human body by the left and right sides, and the transverse plane divides the human body into the upper and lower halves. Image courtesy of: [14]

To create an animated musculoskeletal model with injury capabilities, one has to also study the human body from the biological viewpoint of *anatomy*. The scientific knowledge derived from the study of human anatomy has been one of the great pillars in not only understanding the properties, shape, and structure of the human body but also in the mechanics of human motion. Before delving further, a general definition of anatomy is given that stems from the popular textbook *Gray's Anatomy for Students*:

> *"Anatomy includes those structures that can be seen grossly (without the aid of magnification) and microscopically (with the aid of magnification). Typically, when used by itself, the term 'anatomy' tends to mean gross or macroscopic anatomy-that is, the study of structures that can be seen without using a microscope. Microscopic anatomy, also called 'histology', is the study of cells and tissues using a microscope."* [45]

To summarise the above quote: human anatomy includes both gross human anatomy as well as microscopic human anatomy which known as *histology*. In practice, human anatomy is used synonymously with human morphology [9]. A popular convention used in human anatomy is the classification of human posture into so-called anatomical planes, as depicted in Figure 1. This classification makes it easier when one is describing the anatomy of bipeds and quadrupeds. To give an example, one can group particular flexion and extension positions of anatomical structures for gait analysis. The flexion position of

the knee would be added to the group that represents the set of all positions within the sagittal plane. Because the knee can only be flexed or extended in one degree of freedom it implies that changing the rotation of the lower leg is only possible in the sagittal plane[1].

A useful classification scheme is the grouping of a system of organs where each system performs certain tasks to reach a common goal. This classification, given in [45], defines human anatomy as one group that consists of the following 11 organ systems:

- Integumentary system
- Skeletal system
- Muscular system
- Nervous system
- Endocrine system
- Cardiovascular system
- Lymphatic system
- Respiratory system
- Digestive system
- Urinary system
- Reproductive system

It is worth mentioned that the integumentary system includes the three layers of skin commonly known as *epidermis* (outer layer of epithelial layer), *dermis* (inner connective tissue), and the *hypodermis* that also includes *adipose* tissue (body fat). The muscular system includes *skeletal muscle* that is under the control of the *somatic nervous system* and excludes the other two types of muscles known as *smooth muscle* and *cardiac muscle*. However, skeletal muscles are not the only group responsible for performing movement and the continuous animation of a human character. Take for instance cardiac muscle, which is part of the *autonomic* or *visceral nervous system*. An injury to the heart can immediately cause failure to the mechanics of the heart-muscle, affecting the continuity of the circulatory system, and ultimately disrupting the vitality of a virtual human character.

Injuries to the anatomy mostly affect different systems at once. Work of [89] and [81] tried to describe systems that combine the geometry of organs with anatomical ontologies and injury-penetration probabilities to increase the accuracy of their assessment tools. Anatomical ontologies like [87] are able to provide linked-data on organs and parts of organs. This could be useful where the model only incorporates geometry of complete organs and one wishes to infer damage to parts of an organ or indirect damage to other organ systems. For example, in cases where the model includes one geometrical shape that represents the heart but excludes a geometrical segmentation of parts of the heart, such as the pulmonary arteries that would affect blood flow to and from the lungs. Another possible addition to the musculoskeletal model is the incorporation of a graphical model that relates musculoskeletal injuries on a local level with consequential physical conditions that lie on bodily level. This could support the musculoskeletal model with a rule-based system that can be used when updating static or recorded motions within a kinematic system or generating dynamic motions in a physics-based system. Work of [21] showed that a Bayesian network of thoracic and abdominal injuries that was jointly developed by experts combined with learned probabilities from patient data, shown in Figure 2, was successful in determining most injuries correctly given the conditions of patients.

[1] In case of the knee joint, flexion movements are in the backward (clockwise) direction, while extension movements are in the forward (counterclockwise) direction under the default view to the right of the subject.

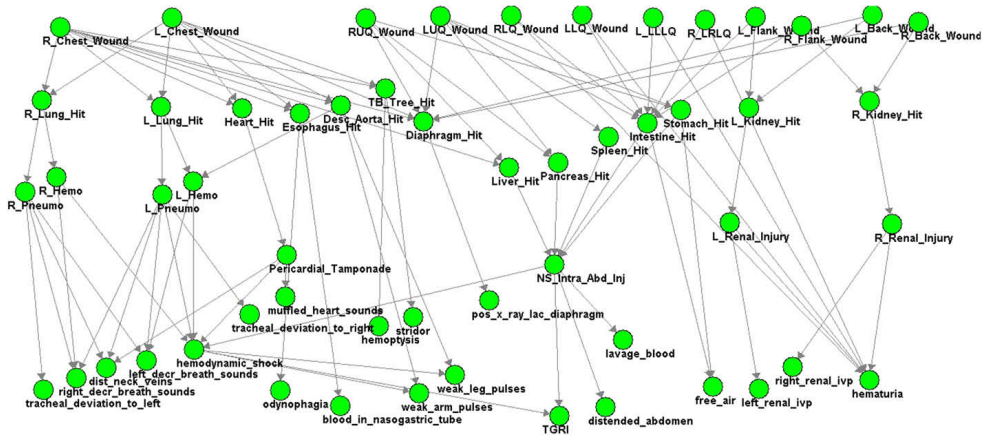

Figure 2: Result of [21] showing the Bayesian network after it was updated with external wound location as an input for their machine learning process (2009).

2.1.1 The Musculoskeletal System

The human musculoskeletal system consists on the one hand of a *skeletal component* that includes bones, joints, ligaments, other connective tissues such as cartilage, and on the other hand the *muscular component* that includes muscles and tendons. Each part will be discussed separately in the following paragraphs, starting first an introduction on connective tissue.

Connective Tissue Connective tissue can be found throughout the body although according to [72] the amount of tissue varies per organ system. Its functions are to store energy, protect organs, provide structural support, connect different tissues, and connect epithelial tissues to muscle tissues. Several types of connective tissue exists, which have been classified. The classification used in this review is taken from [72], which classifies connective tissue into four main classes and several subclasses, as is illustrated in Figure 3. Table 1 gives an overview of locations and functions for several connective tissue types within the mammalian body.

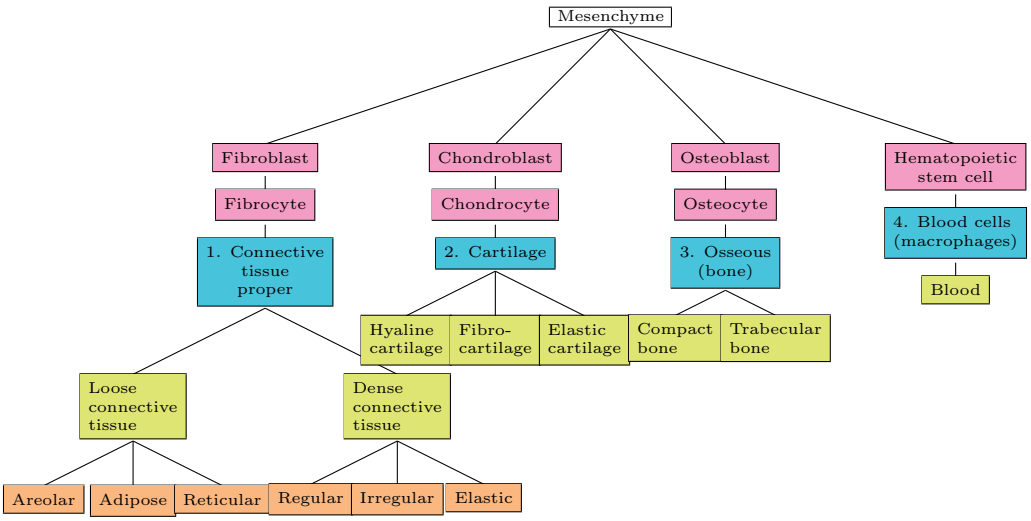

Figure 3: Classification schema of connective tissue with embryonic tissue as the root, also known as the common origin or *mesenchyme*. This is followed by specialised cellular descendants that are subsequently classified into four main classes. Adapted from: [72]

Most types of connective tissue are composed of an *extracellular matrix* that enables the tissue to provide structural support, connect bodies, and protect against both internal injuries, and external injuries such abrasions. The matrix composes of fibres and *ground substance*[2]. [72] states that the amount of combinations of cells with different properties and the composition and arrangement of fibres and ground substance results in the different types of connective tissue and gross structures that are present in the mammalian body.

Tissue type	Function(s)	Locations
Aerolar	*Tissue binding; nutrients transportation and protection to organs and binded tissues; fluid storage.*	*Beneath skin; around muscles, nerves, and blood vessels.*
Adipose	*Energy storage; insulation.*	*Cavities in the body.*
Reticular	*Supporting mesh for soft tissues.*	*Spleen; lymph nodes; liver.*
Regular	*Strong flexible support.*	*Tendons/aponeuroses, and ligaments.*
Irregular	*Great tensile strength in multiple directions.*	*Fascia; periosteum; epimysium; dermis.*
Elastic	*Tissue elasticity.*	*Large arteries; bronchial tubes.*
Hyaline cartilage	*Support; precursor to skeletal bone.*	*Trachea; nose; articular ends of bones; foetal skeleton.*
Fibrocartilage	*Support; absorbing compressive stress.*	*Pubic symphysis; intervertebral discs.*
Elastic cartilage	*Elastic support.*	*Ear; auditory canal; epiglottis.*
Bone	*Framework; protection.*	*Skeleton.*
Blood	*Oxygen, nutrient, hormone transportation; metabolic waste management; body temperature, pH, and fluid volume maintenance; hemostasis; infection prevention.*	*Arteries and veins.*

Table 1: Types of connective tissue together with their functions and locations within the mammalian body. Gathered from: [72], [16], [15], and [17].

Bone This rigid organ of the skeletal system is a form of mineralised tissue that consists for the most part of hydroxyapatite [27], a naturally occurring form of calcium apatite. According to [79], mineralised tissue is responsible for 60% of the bone's weight, while the remaining 40% is divided into 30% for type I collagen and 10% for water. With respect to volume, the distribution is more or less 40% for minerals, 35% for collagen, and 25% for water. On a macroscopic level, bone can be divided into two structures, *compact* (or cortical) and *trabecular* (or cancellous) bone. Compact bone is the outer more denser layer and trabecular bone is the less dense inner layer, as is visible in Figure 4a. With respect to the heterogeneity of bone, [90] states that trabecular bone is found in specific areas such as the vertebral body and at the end-regions of long bones. In contrast to compact

[2]Ground substance is a gel-like substance formed by non-fibrous components of the extracellular matrix.

bone, trabecular bone is highly porous and composes of an extracellular matrix of small rods and plates that are called *trabeculae*, shown in Figure 4b. On lower scales, more structural differences are noticeable. At the microscopic level the *osteon* also known as the *Haversian system*, can be observed. Within compact bone, each osteon is organised in concentric circles containing at the centre the so called *Haversian canals* that help carry blood and other nutrients throughout the bone. Side branches of these canals also spread inter-osteon through small cavities known as *lacunae*. [79] notes that along the boundary of an osteon there are cement-like substances composed of *glycosaminoglycans* that block collagen fibres from linking with other osteons, this blockage lowers the bone's performance to resist mechanical stress and could be considered the weakest link in bone's structure. Within trabecular bone, the small spaces between trabeculae are filled with red bone marrow.

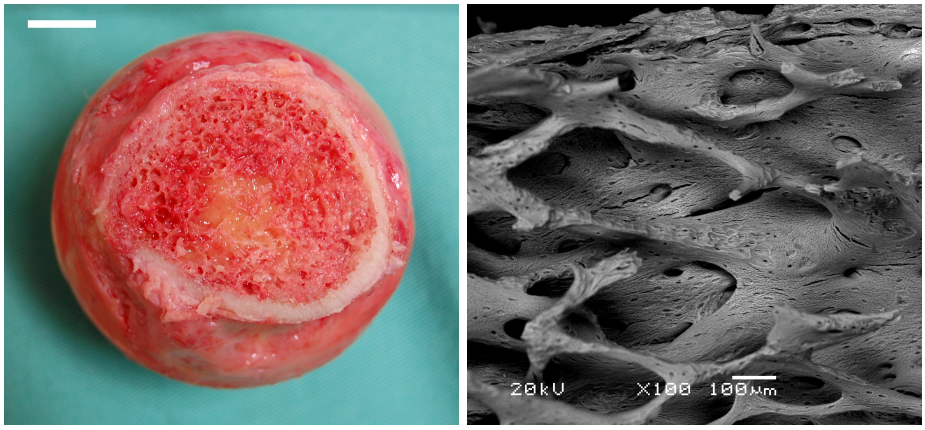

(a) **(b)**

Figure 4: **(a)** - Image of femur head with cortex of compact bone and medulla of trabecular bone at macro level, courtesy of [3]. **(b)** - Scanning Electronic Micrography of deproteinised trabecular bone showing structure at microlevel, image courtesy of [11].

To measure the overall density of bone material, one anthropometrical technique called dual-energy X-ray absorptiometry (DXA) is combined with body size that results in a single scalar known as the bone mineral density (BMD) for a particular bone under consideration. Average BMD can then be benchmarked against standards and used to assess risk of bone fracture for deceases such as osteoporosis. According to [37], the density of compact bone is around 1900 kilograms per cubic metre; of course given the heterogenous nature of bone material, the average densities at macro-levels should be considered as rough approximations.

Joint The joint system works in tandem with the musculoskeletal system, it allows segments to move and rotate independent of one another. It also helps to manage transportation of nutrients and metabolic waste, and provides mechanical support by transferring forces to connected segments and attenuating forces from connected segments. Joints can be classified in different ways. *Gray's Anatomy for Students* [45] adopts a structural classification where joints are divided into *synovial* and *solid* joints. Solid joints are then further divided into two sub-classes, namely *fibrous* and *cartilaginous* joints.

A key characteristic of synovial joints is that segments of bone are not connected directly with solid material. This allows the connected segments to move around freely. The segments are separated by the *synovial cavity* and are indirectly connected via the *synovial lining*, as seen in Figure 5a. The synovial cavity is filled with non-Newtonian fluid that primarily helps in reducing friction between the joint and articulated cartilages.

According to [72], this *synovial fluid* is also contained within the surrounding cartilage. During joint activity the fluid becomes less viscous and expands into the cavity when a joint is under load thereby increasing the cavity's volume for force attenuation. When the load is removed the extra fluid gets absorbed back into the cartilage.

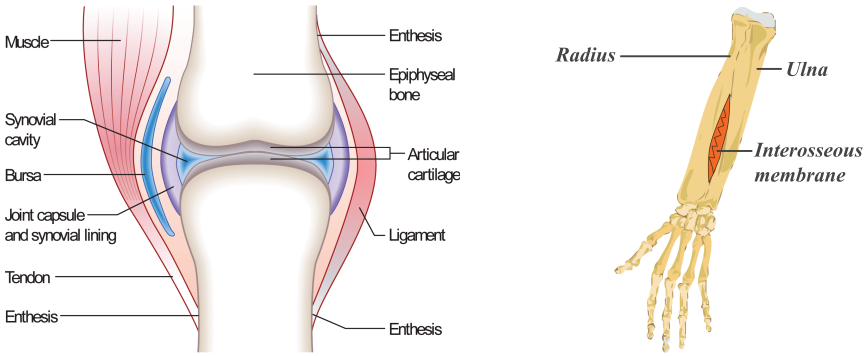

(a) **(b)**

Figure 5: **(a)** - Typical illustration of a synovial joint showing among other things the synovial cavity, the articular cartilage, and the synovial lining that covers the joint, courtesy of [18]. **(b)** - Illustration showing the location of the fibrous interosseous membrane that connects the radius with the ulna in the forearm, adapted from [19].

Contrary to synovial joints, solid joints do connect bone segments directly with solid material. This connection is bridged by connective tissue made out of collagen fibres or cartilage or both (referred as *fibrocartilage*). Fibrous joints have little or no movement, i.e. the interosseous membrane located between the radius and the ulna that is illustrated in Figure 5b. Cartilaginous joints allow for move movement then fibrous joints but less than synovial joints. They are present in areas such as the *epiphysis* regions in long bones of children and between the intervertebral discs.

Ligament Ligaments are a class of strong tissues made from dense collagenous fibres and are viscoelastic. Ligaments extend mechanical support to joints improving its stability (Figure 5a), they help guide joint motion, prevent excessive motion, and provide constant feedback on the relative positions of body parts in physical space. The fibre bundles are primarily aligned with the axis of the ligament with a minority of the fibres aligned in different directions. [79] states that ligaments can therefore sustain large tensile loads from one direction and smaller loads in other directions.

Tendon Similarly to ligaments and joints, [79] states that the function of the tendon are twofold; by connecting muscle to bone, the tendons transmit tensile loads to a bone's insertion point (i.e. distal site) and contribute to the body's posture. This in turn helps to protect the joints from instability. Tendons that are flat and broad are known as *aponeuroses* and are present in areas such as the ventral abdominal, dorsal lumbar, and palmar and plantar regions.

Like the ligament, the structure of a tendon is also composed out of dense connective tissue that is viscoelastic. The majority of the extracellular matrix consists of collagen fibres that are aligned in parallel. In Figure 6, bundles of fibres, the *fascicles*, can be observed. Each fascicle contains specialised fibroblasts of the tendon labelled *tenocytes*. Also apparent in Figure 6 are wave-like patterns have been observed in the fascicles of the tendon. These are known as *crimp*. [44] suggests that crimp could play a role in giving these tissues their limited non-linear (or viscoelastic) properties by allowing strain to take place, elongating the fibres during tensile loads.

Volume wise, [79] states that the extracellular matrix is accountable for 80% of the volume while the cellular portion (containing tenocytes) takes the remaining 20%. The extracellular matrix can be further divided into 55% to 70% of water. The remaining 45% to 30% consists of mostly collagen ([79] states around 60% to 85%), followed by elastin, proteoglycans, and other proteins. Although tendons are part of the muscular component forming the so called *musculotendon unit*, they do not play an active role in the production of motion.

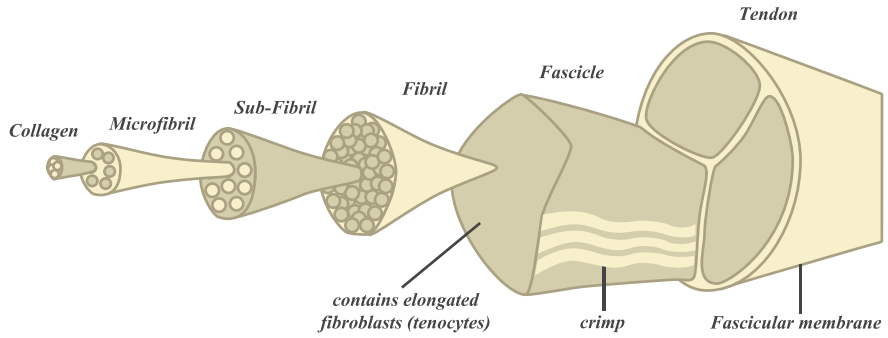

Figure 6: Illustration of the hierarchical structure of the tendon. Adapted from [79].

Muscle Muscles are the actuators of the muscular component and thus do play an active role in the production of motion. They have a similar hierarchical structure compared to tendons, albeit with some key differences. A muscle is sheeted by a layer of connective tissue known as the *epimysium* that also connects with the tendon. The fascicles (fibre bundles) of the muscle are consequently sheeted by another layer of connective tissue known as the *perimysium*, illustrated in Figure 7. Each fascicle consists of fibres, where in case of muscles are long and cylindrical in shape. Next, each muscle fibre is composed of *myofibrils*, the contractile element of muscle. Myofibrils consist of small filaments, the *sarcomeres* that are aligned collinear in a repeating pattern. The sarcomeres are the real actors of muscles and have been described in the *sliding filament model* of [59] and the *cross-bridge hypothesis* by [60]. The ideas can be summarised as follows. When motor neurones receive impulses, calcium flows into the sarcomeres. This triggers the system of *actin* and *myosin* proteins to slide across one another[3]. Along the surface of each chain of myosin there are motor proteins that when triggered extend to grab actin, forming cross-bridges that produce force and effectively pull the actin towards one side. When groups of motor proteins work in concert, the muscle contracts.

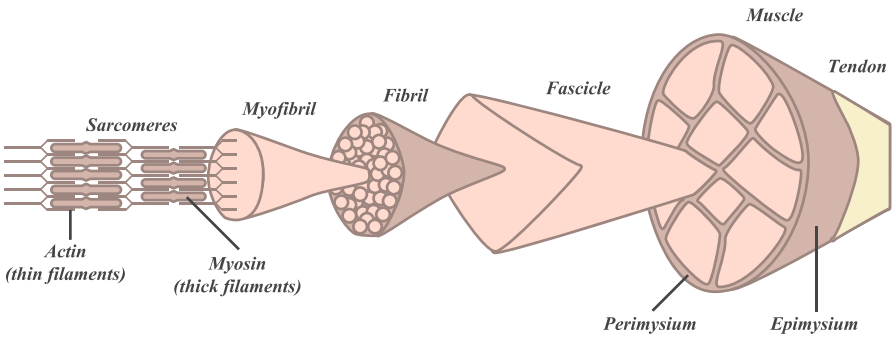

Figure 7: Illustration of the hierarchical structure of the muscle. Adapted from [79].

[3]In order to give a sense of scale, [79] states that actin are approximately 5nm in diameter, while myosin are approximately 15nm in diameter.

With respect to muscle architecture, a variety of muscles shapes exists in the mammalian body that can be differentiated. For instance, [77] classifies five types of muscle shapes, which represent the arrangement of muscle fibres that are not parallel to the longitudinal axis of the tendon that the muscle is attached to. Muscles where its fibres have a different orientation than that of the longitudinal axis are known as *pennate* muscles. The angle that represents the orientation of the fibres is known as the *pennation angle*. Figure 8 illustrates the classes of pennate muscles as defined by [77].

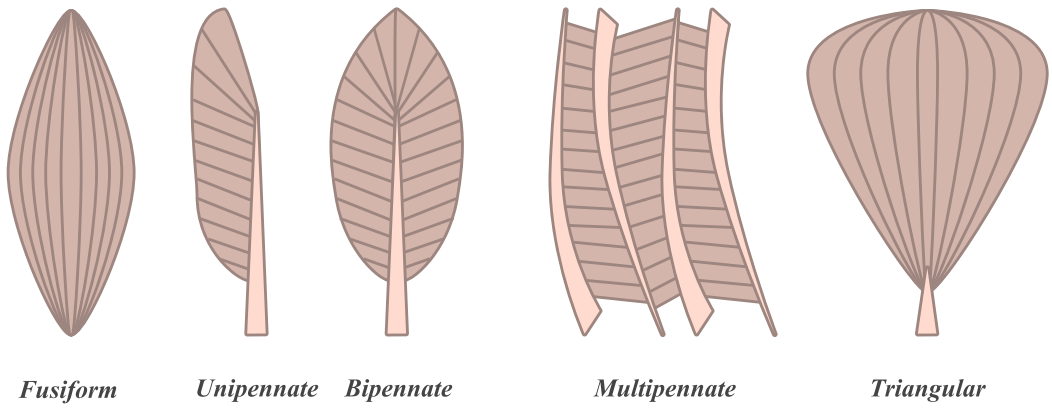

Figure 8: Illustration of pennate muscle types, adapted from the classification of [77].

2.1.2 Anthropometry

Anthropometry is the study of the physical measurements of the human body with the goal of understanding the relationship between different physical characteristics, such as body mass and volume, waist and hip girth, arm length, and stature. What started as a branch of anthropology, [110] states that anthropometry went on to become a useful tool within the fields of human factors engineering and ergonomics. In 1982, [48] published a paper on current developments of virtual human figures. In this paper a reference was made to research carried out by the Boeing company as early as 1968 on what could be the first simulation of a seven-segment articulated pilot character encoded with anthropometric data. In the field of health and medicine, anthropometry is used in the understanding of diseases such as obesity. A global study carried out by [7] validated a new and improved anthropometric measurement index entitled the Body Volume Index (BVI) as a potential replacement to the current Body Mass Index (BMI) measurement standard that is used by health and medical practitioners around the world to measure obesity. A BVI scanner was used by [26] that effectively uses optical light to perform linear scans in order to obtain 120 contours of a scanned subject. The extracted contours are then traced to form a 3D model. An anthropometric analysis is subsequently carried out on the 3D model to infer body shape and body mass composition. An area where body mass composition could be useful for this master project is in scaling the template model in height and body fat percentage (BFP). An empirical study carried out by [57] reformulated equations to predict four-compartment BFP of both men and woman from anthropometric variables that resulted in the following [4]:

$$\mathrm{BFP}_{\mathrm{men}} = 86.010\log(c_a - c_n) - 70.041\log(h) + 36.76 \tag{1}$$

$$\mathrm{BFP}_{\mathrm{women}} = 163.205\log(c_a + c_h - c_n) - 97.684\log(h) - 78.387 \tag{2}$$

[4]The four-compartment model divides body weight (BW) into aqueous (A), protein (P), mineral(M), and fat (F) fractions and is expressed in the form of BW = A + P + M + F, where BW = 1 [55].

where h denotes the height of the subject in inches and c_a, c_h, c_n denote the circumferences of the abdomen, hip, and neck in inches. Using a combination of BFP, the hip-to-waist ratio (HWR) and eight anthropometric variables as sizing parameters, [94] created a displacement synthesiser from scanned subjects that would modify the size and shape of the body accordingly thus visualising areas that would most likely be affected by an increase in BFP, visible in Figure 9.

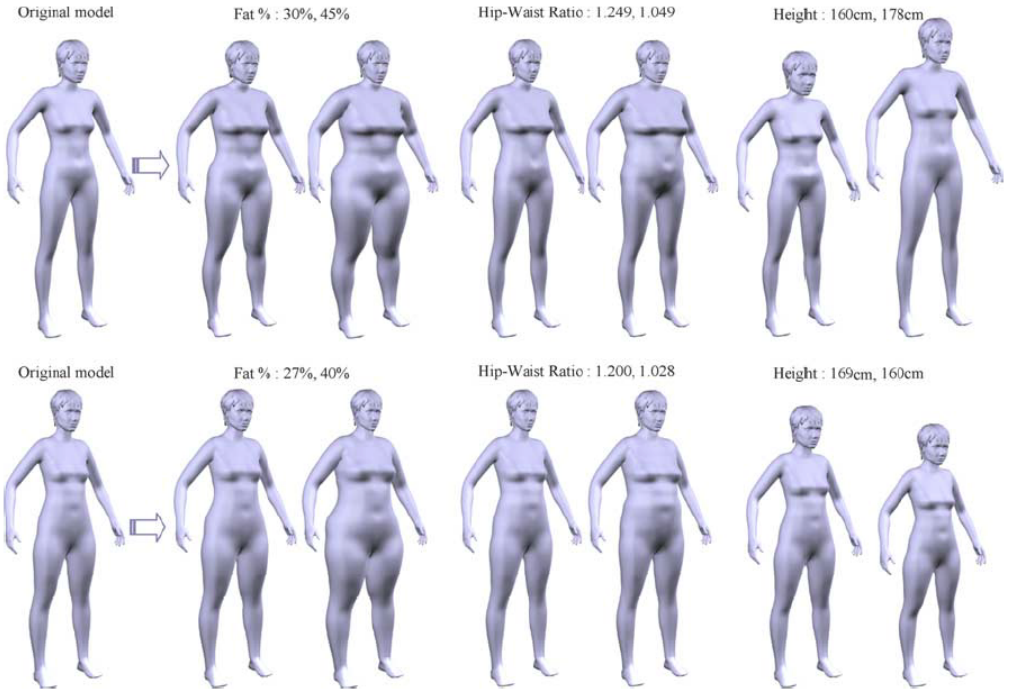

Figure 9: Modification of two subjects by BFP, HWR, and height [94].

2.2 Biomechanics

Articulated motion is a complex process driven by various biological triggers. These triggers lead to the exertion of mechanical forces that in the end are visualised as movements. The role of biomechanics is thus to study the *structure* as well as *function* of biological systems through the lens of *mechanics*.

With respect to *human biomechanics*, the classic book of [110] states that human biomechanics is an interdisciplinary field that describes, analyses, and assesses human movement. Human biomechanics is also intertwined with other fields of movement science such as neurophysiology, exercise physiology, and anatomy. More specifically, the text states:

> *"the biomechanics of human movement has been defined as the mechanics and biophysics of the musculoskeletal system as it pertains to the performance of any movement skill"*[110].

Within the topic of this master project, the role of biomechanics in musculoskeletal injuries starts with a focus on the structure, properties, and mechanics of organic material. These will be discussed in the following sections.

2.2.1 Classical Mechanics

Fundamental understanding of mechanics starts with one of its major subfields. Specifically with the three laws of motion of classical mechanics described by Sir Isaac Newton

in the late 16$^{\text{th}}$ century; starting with the first law, the law of inertia:

1. *An object at rest will remain at rest unless it is acted upon by a force; similarly an object in motion continues to move at constant velocity until acted upon by a force.*

The first law states that when the vector sum of all forces acting on an object is zero then the change in velocity of the object per time unit remains unchanged or stays constant. This can be formally written as:

$$\sum \vec{F} = 0 \;\Rightarrow\; \frac{\mathrm{d}\vec{v}}{\mathrm{d}t} = 0 \tag{3}$$

where $\sum \vec{F}$ is the vector sum of al forces in newton, $\vec{v}$ is the velocity vector in metre per second, and t stands for the time in seconds. The second law of motion can be applied in situations where the previous condition does not hold, i.e. in cases where $\sum \vec{F} \neq 0$, and goes as follows:

2. *The acceleration of an object is proportional to, and in the same direction as the vector sum of all forces acting on the object, but inversely proportional to its mass.*

The second law establishes the relationship between the mass of an object, its acceleration, and vector sum of all forces and can be formally written as:

$$\sum \vec{F} = \frac{\mathrm{d}\vec{p}}{\mathrm{d}t} = \frac{\mathrm{d}(m\vec{v})}{\mathrm{d}t} = m\frac{\mathrm{d}\vec{v}}{\mathrm{d}t} = m\vec{a} \tag{4}$$

where $\vec{p}$ is the linear momentum, the product of mass m in kilograms and velocity $\vec{v}$ in metre per second. Because the second law is only applicable in systems where m remains constant, the term m can be rearranged out of the differential numerator. This leaves the differentials with just the rate of change in velocity per time unit, or the displacement in metres per second per second, and is denoted by the acceleration vector $\vec{a}$. The third law of motion differs in scope with respect to the conditions of first and second laws. Here it makes no difference whether an object is at rest, moving constantly, or accelerating, as the third law defines the behaviour of all forces that are interaction with an object:

3. *For any force that acts on an object there is a reactive force equal in magnitude, opposite in direction, and consisting of a common action line, i.e. they are collinear.*

2.2.2 Statics, Dynamics, and Deformation

The first law of motion is used in a branch of mechanics known as *statics*. In mechanics, statics refers to the analysis of rigid bodies (solids) that are in a state of *equilibrium*, i.e. in the state where a rigid body's acceleration is zero which also means that both net forces (for translational movement) and net moments (for rotational movement) are also zero. The body can therefore be either at rest or having its center of mass move with constant velocity. Studying systems in states of equilibrium are useful to understand what forces are in play or should be taken into consideration. According to [79], statics is generally used in biomechanics to investigate the unknowns in problems that involve the magnitudes of joint reaction forces and muscle tensions.

Dynamics takes the simulation one step further in that it studies how forces and torques causes the state of motion of an object to change, i.e. how a physical system changes over time with respect to applied loads. When forces are exerted on an object, three things can happen, either the object exhibits a change in linear and/or rotational motion, or in the case of dynamic equilibrium, the object experiences a localised shape change over time, a *deformation*. Forces that can be ascribed when an object gets deformed are:

1. *Normal* or *axial*:
    - *Tensile* forces (when an object elongates).
    - *Compressive* forces (when an object shrinks).
2. *Tangential*:
    - *Shear* forces (which in some cases result in bending or twisting of an object).

Because deformation of an object depends also on its material properties, having a quantity that defines the average force per unit area is helpful in approximating solutions for the analysis of intrinsic properties of the object under load. This concept known as *stress* is the amount of force divided by an area of the object. Similarly to the above, two forms of stress are described below, namely *normal* stress σ and *shear* stress τ. The unit of stress is newton per square metre, also known as pressure or pascal. Normal or axial stress can be calculated when the exerted force lies orthogonal to the cross-affected area under consideration. In cases where the exerted force lies tangent or parallel to the affected area under consideration, shear stress can be calculated. Under the assumption that the forces are uniformly distributed along the area and therefore consists of a simple stress pattern, the stress equation can be formally written as:

$$\tau, \sigma = \frac{\vec{F}}{A} \tag{5}$$

where, in this case, A represents the cross-sectional area per square metre. Besides stress, there is also the concept of *strain* that quantifies the normalised amount of deformation after an initial (or referenced) configuration, i.e. the amount of displacement of the intrinsic properties of an object from its original length to its current length (or current configuration). Strain is denoted by ϵ and defines a dimensionless quantity. Similarly to stress it has also two basic forms, which are *normal* and *shear* strain. Normal strain occurs when the displacement happens along the material fibres and is formally written as:

$$\epsilon = \frac{l_1 - l_0}{l_0} = \frac{\Delta l}{l_0} \tag{6}$$

where Δl is the displacement in length and l_0 is the initial length before any deformation occurred. A negative outcome represents a compressive strain, while a positive outcome represents a tensile strain. For shear strains, denoted with γ, deformations made by shear forces are measured. γ represents the tangent between relative displacements of shear forces. The unit is in radians and can be expressed as a decimal fraction, as a percentage, or as parts-per-notation.

Studying the relationship between stress and strain provides insight into the intrinsic behaviour of an object under different load conditions. Figure 10 shows a typical stress-strain diagram of the human cortical bone.

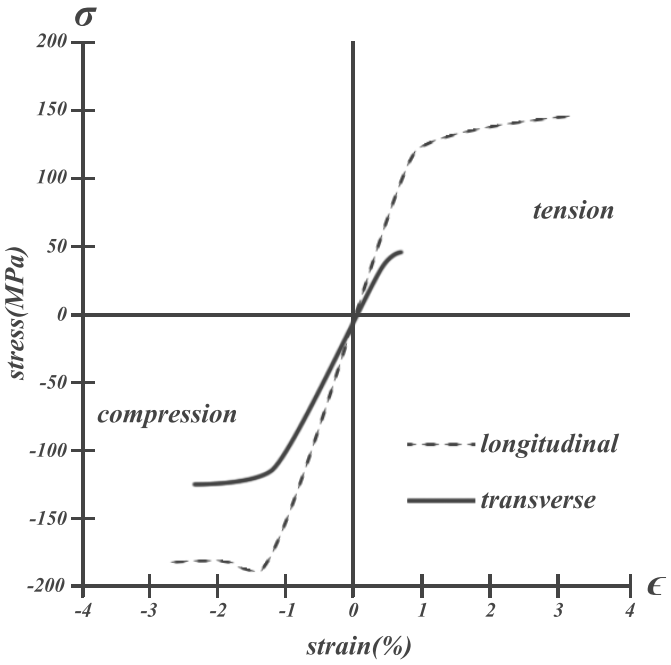

Figure 10: Stress-strain diagram of a typical human cortical bone with strain percentage along the horizontal axis and stress in megapascal along the vertical axis. When forces are exerted in the longitudinal direction instead of the transverse, the material can withstand more stress before it reaches the point of failure, characterised by the longer dotted graph in the figure. Also apparent from the figure is the toughness of the cortical bone material during compression when compared to tension. Remastered from: [51].

When an object experiences tensile or compressive forces in one direction it can contract or expand in other directions that lie orthogonal to the direction of applied forces. This characteristic is known as the *Poisson effect*. The effect can be measured by taking the ratio between the change in normal strain with the change in shear strain and is referred to as *Poisson's ratio*, which is denoted by ν. Formally it is written as:

$$\nu = -\frac{\mathrm{d}\epsilon_n}{\mathrm{d}\epsilon_s} \tag{7}$$

where ϵ_n and ϵ_s denote the normal and shear strains respectively.

2.2.3 Elasticity and Plasticity

A deformed object is considered *elastic* when it deforms back to its original configuration after the applied load is removed and *plastic* when at least parts of the deformation are permanent. The graph in Figure 11 illustrates a stress-strain curve of a hypothetical object that experienced different tensile forces[5]. The numbers along the curve in Figure 11 represent several known characteristics that play a key role in the analysis of the material.

[5]The graph shows only one curve, however in reality different stress-strain curves exists when different forces are exerted on the same material and in different environmental conditions. In addition, there are also distinctions between a *true* stress-strain diagram and an *engineering* stress-strain diagram.

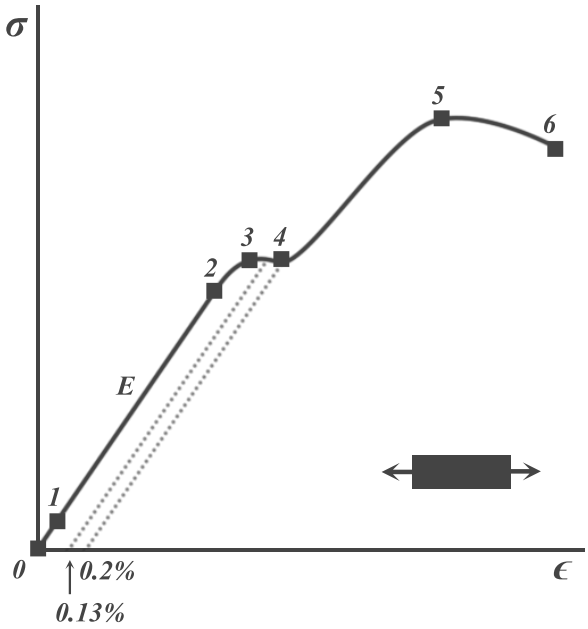

Figure 11: Engineering stress-strain diagram for illustration purposes, showing key characteristics of a hypothetical elastic-plastic object that experiences different tensile forces.

Point *0* in Figure 11 represents the initial configuration, when no forces are exerted on the object. The first point on the curve, point *1*, represents the *true elastic limit*. Between point *0* and *1* no dislocations are visible on the atomic level or molecular scale. Point *2* represents the *proportionality limit*, after this point the elasticity of the material does not behave linearly. The segment of the curve between point *0* and *2* is said to be linear-elastic or Hookean implying a conformance to *Hooke's law*. The principle of Hooke's law, which in mechanics is used for models such as springs, can be described in terms of material functions of stress and strain for both normal and tangential forces:

$$\sigma = E\epsilon, \tag{8a}$$

$$\tau = G\gamma \tag{8b}$$

where E denotes the elastic modulus or *Young's modulus* for normal forces and G denotes the shear modulus or *modulus of rigidity* for tangential forces. Young's modulus is representative for the *stiffness* of a material, the higher the elastic slope, the more stiffer the material. Point *3* represents the *elastic limit*, also known as the *yield strength* or *yield point*[6]. The segment between point *2* and *3* defines the complete elastic behaviour of the material, removing any load that falls within this segment would allow the material to deform back to its original configuration. After this point, the material behaves plastic and any further deformation is considered permanent. One technique to quantify plastic deformity is mentioned in [79] and is illustrated in figure 11. In this example, the load that is applied on the object is removed at the point on the curve between *3* and *4*. The dotted line represents the linear regression of the elastic deformation with the same Young's or rigidity modulus that eventually intersects the strain axis. The intersection point on this axis is called the *plastic strain* that quantifies the amount of permanent strain, in this example 0.13%. Point *4* represents the *offset yield point* that can be derived using the offset method. The offset method is used for cases where it is difficult to measure the exact point when the material yields. Similarly to the previous derivation of plastic strain, the

[6]The yield strength or yield point represents the starting point of plastic deformation.

method works by drawing a line, which according to [86] starts generally with a strain offset of 0.1% to 0.2%, and progresses in parallel with the linear-elastic segment of the curve. The intersecting point *4* between this line and the original curve is considered the offset yield point. Point *5* on the curve represents the ultimate tensile strength of the material followed by point *6* that represents the rupture point of the material; when the object finally fractures. An overview with some mechanical properties for three biological materials is shown in Table 2.

Material	Ultimate Strength (MPa)	Modulus (GPa)	Elongation (%)
Compact bone	*100-150*	*10-15*	*1-3*
Trabecular bone	*8-50*	—	*2-4*
Tendon, ligament	*20-35*	*2-4*	*10-25*

Table 2: Mechanical properties of three biological materials, compact bone, trabecular bone, tendon, and ligament. Adapted from: [95].

2.2.4 Viscosity, Viscoelasticity, and Hyperelasticity

Before proceeding with the concept of *viscoelasticity*, a clear definition of *viscosity* is in order. Viscosity is usually denoted by η and applies to fluids. It is the measurement of resistance against deformation that takes place within a fluid, more specifically the resistance to shear and tensile stress. If the exerted forces being applied on the fluid are continuous then the deformation is also continuous. This continuity in deformation is known as *flow*. However, the time dependency of viscosity implies that as soon as the exerted forces are removed, the deformation is gradual until the fluid reaches a state of equilibrium.

Viscoelasticity applies to materials that inherent both properties; elasticity for solids and viscosity for fluids. Viscoelastic materials thus distribute strain energy in two ways, the elastic component stores it as potential energy and the viscous component dissipates some of in other forms of energy such as heat and sound. [79] states that almost all biologic materials behave viscoelastically. Because of this loss of energy, viscoelastic materials take a different path that requires less energy when recovering towards their initial configuration. This property is known as *hysteresis*. In terms of stress and strain, the amount of energy lost is equal to:

$$\int_0^p \mathrm{L}(\sigma)\mathrm{d}\sigma - \int_p^0 \mathrm{U}(\sigma)\mathrm{d}\sigma \tag{9}$$

where $\mathrm{L}(\sigma)$ and $\mathrm{U}(\sigma)$ are functions of loading and unloading strain having stress as their input. p denotes the peak load. Visually, this can be represented by loading and unloading curves that form a loop as illustrated in Figure 12.

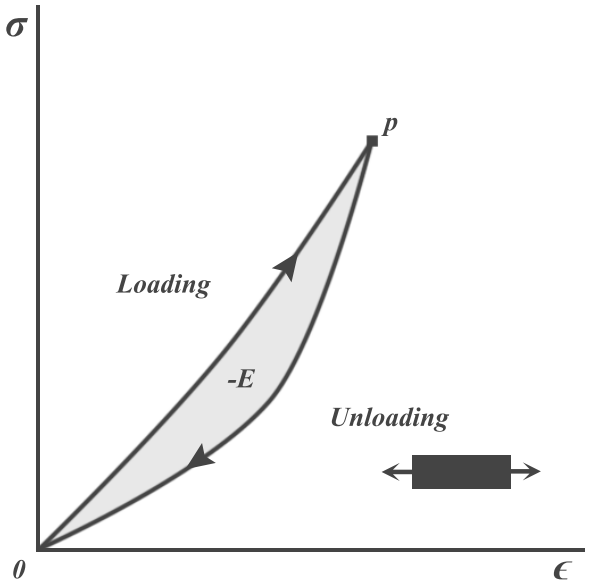

Figure 12: Stress-strain diagram of a hypothetical viscoelastic material showing hysteresis during one tensile loading and unloading cycle. E denotes the energy dissipated through e.g. heat and sound (not to be confused with Young's modulus), and p denotes the peak load. A minus sign is added by convention to denote dissipation (loss) of energy.

The time-dependency that comes with a viscoelastic material gives these type of materials the characteristic that the amount of deformation is dependent on the non-linear rate of forces that are exerted on the material. Another phenomenon of viscoelastic materials is *creep* that characterises the time-dependent accumulation of strain under constant stress, i.e. a gradual deformation and recovery as seen in Figure 14a. The inverse of creep phenomena is known as *stress relaxation*. This characterises the behaviour of stress under a constant strain for viscoelastic materials, shown in Figure 14b.

Hyper-elasticitiy applies to a particular type of material referred as a *cauchy-elastic* material that can undergo large non-linear elastic deformations. Similarly to the above, this type of elastic behaviour can also be modelled constitutively. Two of the most popular models are the *neo-Hookean* mechanistic model and the *Mooney-Rivlin* phenomenological model. Figure 13 shows a stress-strain diagram of a couple of hyper-elastic models.

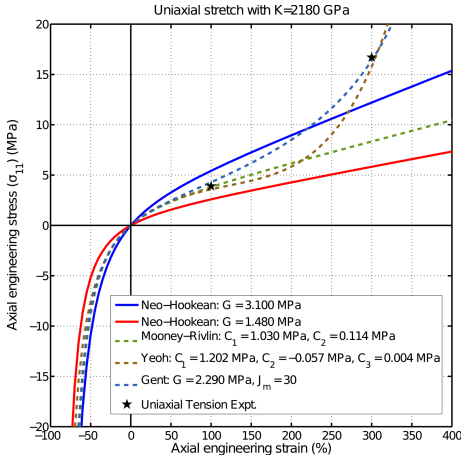

Figure 13: Stress-strain diagram showing different hyper-elastic models. Courtesy of [5].

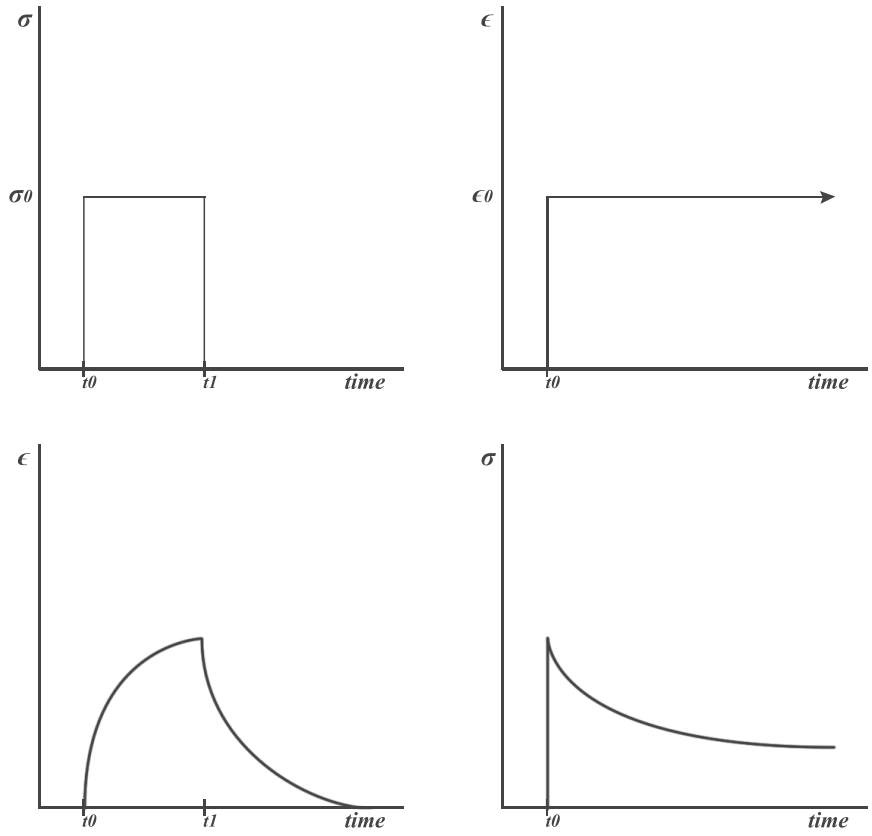

(a) **(b)**

Figure 14: **(a)** - Separate stress-strain diagrams with respect to time showing creep for a solid viscoelastic material. Applying instantaneous stress translates into gradual deformation. **(b)** - Separate strain-stress diagrams with respect to time showing stress relaxation for a solid viscoelastic material. When the strain remains constant, stress levels relieve gradually.

2.3 Soft Tissue Deformation & Musculoskeletal Modelling

This section reviews work that has been carried out on musculosketal modelling and soft tissue mechanics.

2.3.1 Soft Tissue Deformation and Simulation

In human physiology, [72] defines the term *tissue* as a group of cells that share the same functions, which are to give support, protection, and connectedness to structures, organs, and bones in the body. Within this broad group of cells, the sub-term *soft tissue* refers to the cell groups of muscle, fat, fibrous tissue, blood vessels, or other supporting tissue of the body according to official terminology of the National Cancer Institute of the United States of America [13].

From a mechanical perspective, soft tissues exhibit an elastic and plastic response when forces are applied. One way to model these affects is to subdivide (or discretise) the inner-space or inner-volume of a soft body into smaller elements so that forces can be applied to each element separately and interaction between the elements can also be modelled physically. According to [99], in the past decade these physical consistent models for soft tissue deformation that were based on equations from nonlinear continuum mechanics

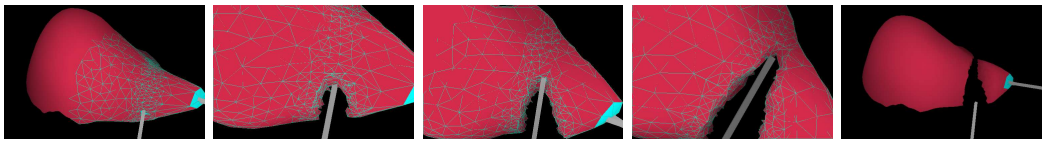

Figure 15: Result from [84] showing simulation of an invasive hepatic surgery simulator. They used a linear-elastic FE model that includes the notion of anisotropic deformation, or more specifically, the behaviour of a transversally isotropic material, where different stiffness properties of the material are defined in a given direction (2002).

were well established. New applications such as real-time surgical training would use models such as [41, 97, 84, 42, 113, 114] that applied finite element analysis (FEA) to numerically solve the problem with the finite element method (FEM) or finite volume method (FVM). Figure 15 shows work of [84] that a linear FE model anisotropic-like behaviour for surgical training of laparoscopic procedures. Advancements in this area led to the creation of the total Lagrangian explicit dynamics (TLED) finite element algorithm that uses a total kinematic framework of shape functions with spatial derivatives. One example is the TLED-FE model from [73] that precomputes spatial derivatives offline before the time-step procedure thereby lowering the runtime cost with approximately 35% fewer floating-point operations per element. In addition, it was possible to port explicit FE models to the GPU due to the use of an explicit time integration scheme that allowed parallel execution to be a practical possibility. For instance, one implementation by [98] ported the complete integration scheme unto the GPU by loading elements as texture arrays. Their approach reached simulations with approximately 160.000 linear tetrahedral elements with up to 10.000 degrees of freedom in real-time.

In computer graphics, techniques for both rigid and soft deformation was already an active area of research that started with the pioneering work of [103] and [102], which introduced models based on elastic theory. In the past decade, interesting solutions to geometric problems such as cutting and splitting of meshes were introduced. One idea that is still widely used today is the dynamic use of multiple resolutions or remeshing in areas where more detail is required, such as along the boundary of a split mesh. Multi-resolution techniques, such as [50] and [31], were further developed to cope with shortcomings such as large numbers of subdivided tetrahedra, referred as *the fragmentation problem*, and badly shaped slivers known as *degenerate tetrahedra*. Regarding the fragmentation problem, [30] used a state machine model to track topological changes and control topological patterns. The algorithm continuous progressively, subdividing tetrahedra when subdivision-rules are not a met. Besides keeping the number of new elements low, the state machine also allows reverse movements and can therefore represent true arbitrary cuts. For both fragmented and degenerate tetrahedra, [49] modified their remeshing technique by introducing edge-collapse. Edge-collapse solves the problem by computing the quality of a tetrahedron with the ratio of its inscribed sphere to the radius of its circumscribed sphere. When the quality reaches below a certain threshold τ, the shortest edge from the set is removed and the data-structure is updated. With respect to conservation of mass, [49] also showed experimentally that degenerate tetrahedra chosen before collapsing edges have an almost zero volume within the mass-spring system and can therefore be neglected. However, remeshing still had problems numerical instabilities present in spring-relaxation schemes and performance degradation according to [78]. [96] and [83] therefore tried to eliminate polygonal meshes completely and developed a complete mesh-less approach using implicit surfaces. The surfaces, defined by nodal shape functions, were sampled adaptively allowing cuts and fractures to be visible.

2.3.2 Musculoskeletal Modelling and Representation

Modelling and representing the musculoskeletal system is a complex problem due to the inherit properties of soft tissues. [66] provided an extensive survey on musculoskeletal modelling of which some of the literature is presented here and complemented with other work and more recent findings.

On of the early approaches in modelling muscle deformation was [38]. It introduced a multi-layer approach for human character animation that included representations for muscle and adipose tissue. Bulging and other physical effects were achieved with the use of free-form deformation (FFD) lattice. Figure 16a shows the result of their proposed animation system. [64] also used FFD with Bézier surfaces for the synthesis of human skin. [104] developed a human model based on B-splines and meta-balls. They used ray-to-surface intersects to sample points on the surface of each meta-ball. These sample-points where then used as control-points for the B-splines to generate a smooth skin surface. The meta-balls are attached to the armature and therefore represent the gross anatomy of the model and the input for *skinning*[7]. Skinning came its share of side-effects when blending animated characters into certain poses, for example the collapsing-elbow problem as mentioned in [70]. To try to solve these class of problems, [70] developed their semi-automatic pose-space deformation framework that improved interpolation of the shape functions, albeit manual intervention was still a requirement. For example, to get the desired amount of muscle bulge, constraints would be manually introduced to control and animate the amount of deformation in separate pose-spaces. Later [22] applied the same approach for an anatomically based human hand model.

[109] instrumented a more direct approach using primitive cylinders for muscle representation that are attached to two origin and two insertion points of specific bones. This gave an added layer of biological realism due to the fact that more origin and insertion points may lie on different bones and segments. The inner action-line of each deformed muscle-cylinder is divided into several cross-sections and includes extra position-constraints for easier placement around bones and joints, visible in Figure 16b. Deformation of each muscle is performed by scaling the width and the thickness dynamically based on the ratio between the current length of the muscle and its rest length, thus preserving volume. Similarly, [91] used ellipsoids for their muscle representation shape due to the inherent property of an ellipsoid to scale along its principal axes, shown in Figure 16c. The scaling of these fusiform muscle-shapes allowed volume to be preserved for both *isotonic* and *isometric* contractions.

While practical for real-time applications, the simple models used in earlier work have their limitations when it comes to simulating the physical and biological mechanics and when one wants to obtain a more accurate model that incorporates physiological properties. As [20] states:

> *"Considering the variety of muscle shapes and differences in functionality, simulations with over- simplified or idealised muscle geometry and biomechanics will not give satisfactory results, especially when trying to examine a group of cooperating muscles in action."* [20]

Using physics-based techniques such as mass-spring systems can add one extra layer of biological accuracy and realism. One of the early physics-based approaches was [68]. They presented a methodology to automate the animation of facial expressions with a three-layered mass-spring system included in a biomechanical tissue model. The model used triangular prism elements, where the three layers connected with springs, represented the epidermis, dermis, and muscle layer that eventually connects to nodes on the surface of the skull.

[7] "Skinning" is the more casual term for skeleton-subspace deformation (SSD).

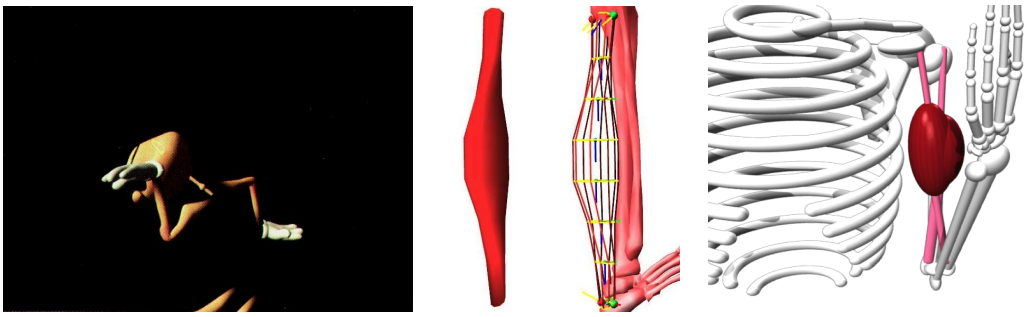

(a) **(b)** **(c)**

Figure 16: (a) - Result from [38] showing the kinematic fore-arm bulging (1989). **(b)** - Work from [109] showing a deformed cylinder attached via the four origin and insertion points, visualised by the red-green spheres on the top and bottom respectively. The yellow polylines visualise the eight cross-sections of the muscle (1997). **(c)** - Work from [91] showing the biceps brachii fusiform ellipsoid-muscle getting bulged while flexing (1997).

Regarding mass-spring systems used specifically in muscle models, [76] introduced a different type of spring, so-called angular springs to control the curvature along the surface of a muscle mesh with two-dimensional coefficients. Figure 17a shows the result of compression on the bending and twisting of vertices with and without angular springs. Contractile forces were calculated with inverse-dynamics based on the length of the action-line. The position of each surface-vertex corresponding to a node was modelled with the following Lagrange equation:

$$m_i \frac{\mathrm{d}^2 \vec{x_i}}{\mathrm{d}^2 t} + \gamma_i \frac{\mathrm{d}\vec{x_i}}{\mathrm{d}t} + \mathrm{f}_{result}(\vec{x_i}) = f_{external_i} \tag{10}$$

where m_i and γ_i are the mass and damping factor of node i, and $\mathrm{f}_{result}(\vec{x_i})$ and $f_{external_i}$ are the derived result and external forces. The approach got extended by [25], where an action-line is not a straight line but a one-dimensional spring for fusiform muscles and a two-dimensional spring for flat muscles that consist of more than one action-lines. Furthermore, they incorporated attractive and repulsive force fields, using ellipsoids, to control the trajectory of the action-line and prevent collision with the skeleton. However, no muscle-to-muscle collision was included. Springs were also used by [67] to represent three points along a quadratic Bézier action-line curve, shown in Figure 17b. A fusiform ellipsoid is used to represent the muscle volume where a parameter for the girth controls the muscle's bulge size and a taper parameter controls the curvature at the attachment points approximating tendons. [118] looked at the motion of breathing and simulated respiratory-mechanics using approximately 1500 mass-spring nodes for the upper torso that included both soft and rigid bodies, shown in Figure 17c.

Simulating biomechanically accurate muscle models also drew interest into using the finite element method (FEM). Early work of [39] used FEM in combination with forward dynamics to simulate movement driven by muscle forces. Non-linear forces were applied to the three-dimensional FE model that was comprised out of four twenty-node iso-parametric brick elements. [117] also used FEM to perform biomechanical muscle deformation. The linear-elastic model was coupled with a hierarchical voxel-based mesh of the gastrocnemius muscle of a frog. To validate the model, tension-length curves were plotted to compare isometric with normalised length, and Gasser and Hill's quick-release experiment was simulated to examine velocity dependency inherent to the muscle. However, in both cases only small deformations were possible due to the linear-elastic assumption in their models.

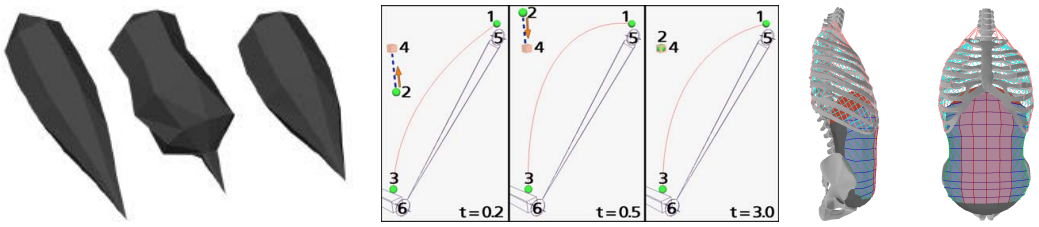

(a) **(b)** **(c)**

Figure 17: **(a)** - Work from [76] showing the muscle volume in rest state (left), under compression without angular springs (middle), and under compression with angular springs (right) (1998). **(b)** - Work from [67] showing three control-points of the quadratic Bézier action-line curve and a fourth point for a user-defined constraint (2007). **(c)** - Work from [118] showing rigid bodies in light gray shades and deformable surfaces in shades of rust, pink, and blue. The model contains approximately 1500 mass-spring nodes (2004).

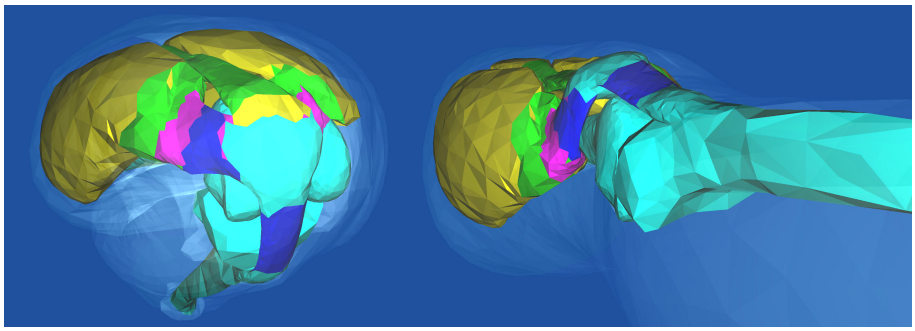

Figure 18: Result of [56] showing a tetrahedral mesh of the knee that contains around 10.000 nodes, 10.000 triangular elements, and 40.000 tetrahedral elements. The left image shows the knee in flexed-position while the extended-position is shown on the right. Colours are given to different regions of each tissue type. (2001)

Non-linear elasticity, on the other hand, allows larger and complex deformation-behaviour to be possible. [56] applied implicit FEM to non-linear behaviour, making way for a collision-free method that deformed a section of a model from the Visible Human dataset. Figure 18 shows one result combining different tissue types into the model. [69] also used non-linear finite element analysis (FEA) to produce realistic deformation of muscle that accommodated different fibre arrangements. Similarly, recent work from [33] tackled the same problem of accuracy by creating a new FE model that not only handled different fibre arrangements but also defined fibre geometry on a per-bundle basis using Bézier splines. Four different templates of typical muscle architecture were used to dictate the behaviour of a set of fibres defined as a set of splines. Intermediate splines within each set were computed as follows:

$$\mathrm{b}_i(s) = \begin{cases} \mathrm{b}_i^a + \left(1 - \frac{s}{f}\right)(\mathrm{b}_i^b - \mathrm{b}_i^a) & \text{when } 0 \leq s \leq f \\ \mathrm{b}_i^a & \text{when } f < s < \infty \end{cases} \tag{11}$$

where b_i denotes a Bézier spline, b_i^a and b_i^b are the two boundary splines, s denotes the control-points for intermediate splines, and f denotes the number of fibres. By grouping splines together, each set of splines can be used as a representation for fibre bundles, as shown in Figure 19. The visible geometry of the fibres were represented as polylines sampled from each spline.

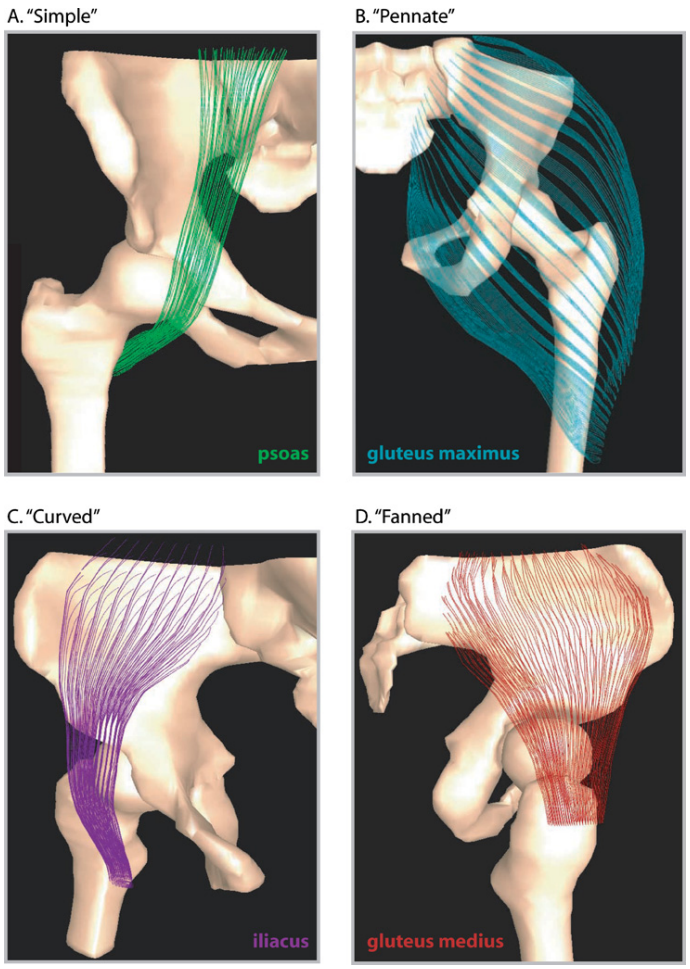

Figure 19: Result of [33] showing the four muscle architecture templates consisting of parallel, pennate, curved, and fanned shapes of fibre bundles. The sampled fibre geometries are mapped to the (A) psoas, (B) gluteus maximus, (C) iliacus , and (D) gluteus medius muscles respectively (2005).

More recently, [29] developed a real-time co-rotational FE model driven by both isometric and isotonic forces from Electromyography (EMG) readings. They demonstrated a solid performance of 45 frames per second for a volumetric model composed of 7128 tetrahedrons. Next to the vast amount of FE-based implementations, there are also notable work that incorporated the finite volume method (FVM) for the modelling of musculotendons. Having the advantage of being more simpler and intuitive to implement [100] and [101] developed transversely isotropic, quasi-incompressible, and hyper-elastic FV models. Although FVM requires less computation and memory management in general, it is a zero-order based method and therefore less accurate when compared to FEM, which could lead to more incorrect results during the simulation.

2.4 Musculoskeletal Injuries

In order to simulate musculoskeletal injuries, one has to first describe and assess the different kinds of injuries that can be inflicted. Because injuries are classified in several ways such as [1] and [2], it is suitable to first establish a classification scheme for consistency reasons. Due to the goal of this master project to simulate musculoskeletal injuries in real-time, it is convenient to classify the injuries based on their anatomical location. Therefore, the classification adopted for this review is taken directly from the Field Medical Training Battalion (FMTB) of the United States Marine Corps [28], which classifies the following

types of injuries:

- *Abrasion*: a superficial scratch of the skin's surface.
- *Laceration*: a cut (can be smooth or jagged).
- *Avulsion*: an injury where flaps of skin are torn loose or pulled off completely.
- *Amputation*: removal of a limb or other appendage of the body.
- *Strain*: injury to muscles or tendons from over stretching or overexertion.
- *Sprain*: joint injury (leads to partial tearing or stretching of supporting ligaments).
- *Dislocation*: bone displacement (leads to stretched ligaments around a joint).
- *Fracture*: break in bone continuity (classified as a closed or open facture).

It is important to note that this classification scheme relates to the damage that has been inflicted and does not directly infer to the external mechanisms that lead to an injury in the first place. The following subsections discusses each type of musculoskeletal injury coupled with work on musculoskeletal injury simulation.

2.4.1 Abrasion

Abrasions are superficial scratches along the skin's surface or epidermis layer. [28] also refers them as *brush burns*, *mat burns*, and *road rash*. In the field of computer vision, the detection of skin injuries has been studied with automatic image segmentation techniques such as [23] and [115]. These have shown to accurately detect common and cancerous lesions based on photographs of a patient's skin. [106] and [107] focused on the repair and remodelling phases of skin injuries using numerical techniques and continuum models, while [61] focused on radial heat flow throughout dermal tissues. Regarding the actual simulation of an abrasion, no research has yet been found with this goal in mind. This is probably due to the fact that abrasions are considered mild injuries and are therefore easily treated. Another possible cause is the widespread use of standardised techniques such as texture and displacement mapping [24] for real-time applications that lend abrasions to be easily visualised in interactive settings.

2.4.2 Laceration

A more severe injury than an abrasion is a laceration, which is a cut spreading through the surface of the skin. The guideline in [28] mentions that it can be a smooth or jagged cut and is caused by an object with a sharp edge or as a result from severe blows or impacts with blunt objects. One of the first breakthroughs tackling the problem of laceration in an interactive setting were [50] and [31]. They used a hybrid approach combining mesh and mess-less models to simultaneously improve computational performance when modifying the topology. Both used mass-spring models defined on top of a mesh-based tetrahedral decomposition within the volume of the object. During cutting they subdivide and replace intersected tetrahedra with non-intersecting ones thus increasing the level-of-detail at the proximity of the surgical tool, also known as *remeshing*. This is followed by updates to the cached data-structures storing the vertices. Figure 20a shows the replaced tetrahedra with higher resolution along the discontinuity of a square-shaped object. Prior to this breakthrough, anatomically accurate models such as from [88] and [62] used the finite element method (FEM) that directly approximates equations of continuum mechanics for surgery planning. Although more accurate by default, these were at the time not computationally feasible for use in interactive applications. [35] and [41] were able to achieve interactive frame-rates by including a pre-processing stage and using a smaller set

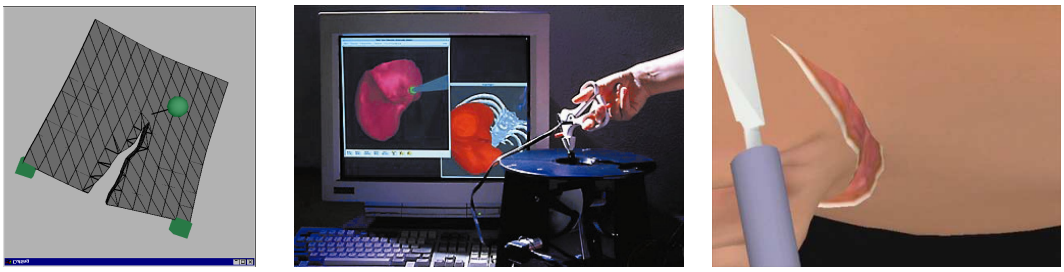

(a) **(b)** **(c)**

Figure 20: **(a)** - Work from [50] showing a square-shaped object cut while two forces pull in opposite directions (2000). **(b)** - Work from [41] showing a surgeon manipulating a force feedback device. When collision is detected with the surface of a virtual organ, the mesh is deformed and a nonlinear reaction force is computed and sent back to the force feedback system (1999). **(c)** - Work from [93] showing the interactive incision process for a face-lift surgery simulation (2006).

of elements. [41] also attached a haptic device for force feedback thus improving realism and immersion of the simulator, as shown in Figure 20b. However, due to the dependency on the pre-processing phase for the interactive FE models, topological modification was not possible.

Figure 20c shows another approach by [93] for simulating laceration. Their approach encodes results of offline FE computations into a four-dimensional discontinuous free-form deformation model adapted from [92]. The framework is extendable allowing the model to simulate arbitrary cutting patterns. However it does not take other organ systems such as the skeleton into account. Another drawback lies in the nature of the free-form deformation technique, which is confined to the iso-parametric manifold of the mesh thereby rendering the technique unsuitable for injuries such as avulsions.

2.4.3 Avulsion

Avulsions are injuries where flaps of skin are torn loose or completely pulled off exposing underlying structures such as fat, musculotendons, and bone tissues. Simulating avulsion can be seen as an extension to the body of work that has been carried out on lacerations. [71] used an extended FE model to allow skin to be treated as a separate layer during inter-element cutting. Elements that lie on the boundary or "skin" surface are duplicated and constrained with respect to their allowed displacements. As the cutting-object translates forward across the interlayer boundary, the displacement constraints are removed in a progressive manner, seen in Figure 21a. The duplication technique is made possible by using an augmented system similar to [43] that includes three Lagrange multipliers to represent the necessary forces that satisfy the displacement constraints. This allows topological changes to be visually represented without having to re-factorize the stiffness matrix. A simpler technique when comparing it to the virtual node algorithm of [74] where continuous updates are required thus increasing computation time. True mesh-less models such as [96] and [83] used sampling technique to control the disconnection between particles representing the mesh-less discretised layer. [96] demonstrated flaps of an apple's skin deforming naturally until falling off with their non-uniform adaptive sampling technique, shown in Figure 21b.

Within the interdisciplinary field of biophysics, avulsions have been of interest to plastic surgery training simulators. For facial reconstruction and inguinal herniotomy, [65] experimented with hyper-elastic models for human skin and used the result in a dynamic explicit FE analysis for use in a prototypical real-time simulator. They compared the

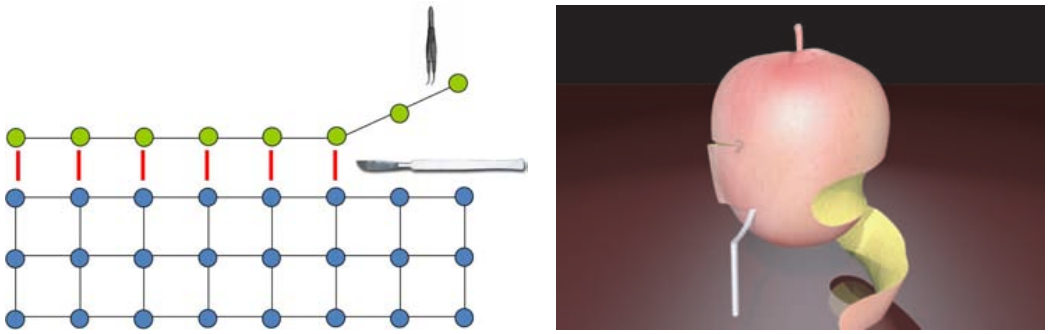

(a) **(b)**

Figure 21: **(a)** - Work from [71] showing the duplicated surface elements during an undermining procedure separating subcutaneous tissue from skin. Also notable is the virtual forceps (top right) that introduces tension (2007). **(b)** - Work from [96] showing an apple, consisting of 2121 particles and 6124 faces, being peeled at 25 frames per second. The skin of the apple deforms until it eventually falls off (2006).

real-time performance of their hyper-elastic model on both the CPU and GPU, where the GPU-based implementation handled around 50.000 elements above 1.000 frames per second, while the CPU-based implementation reached around 500 elements for the same frame-rate.

2.4.4 Amputation

An amputation is defined by the removal of a limb or other appendage of the body, exemplified in Figure 22, which shows an amputated cartoon character from work of [80]. [28] categorises amputations into surgical or traumatic. On the contrary to what some may believe, most amputees don't experience severe blood loss. This is due to the elasticity inherent in blood vessels. Nonetheless, amputations are severe injuries causing extensive damage to combined organ systems within the body. From a geometric and modelling perspective, such injuries entice the need for an efficient collision strategy for the decomposition scheme to separate each bounded volume and conform to the non-linear boundary conditions. Collision techniques such as in the seminal work of [34] for cloth simulation could be useful for interference-free collisions of soft-bodies. Once the volumes are displaced in non-intersected configurations, the simulation would require similar FEM as was discussed in previous sections of this review.

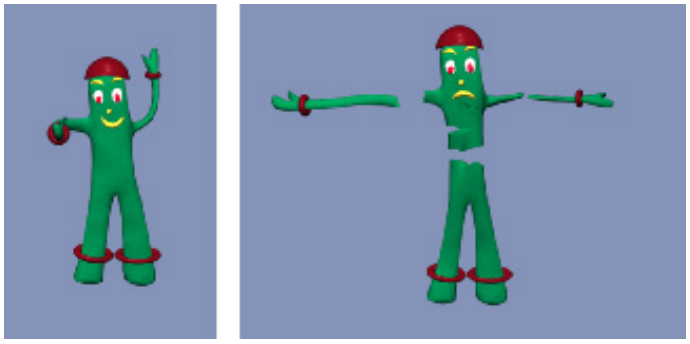

Figure 22: Amputated cartoon character simulating ductile fracture from [80] (2002).

2.4.5 Strain

Not to be confused with mechanical strain, the description in [28] defines strain as an injury to a muscle or tendon as a consequence of over-stretching or overexertion within its tissues. Thus, understanding mechanical strain distributions and how musculotendons generate force plays an important part in the successful modelling of strain (and strain-like) injuries. [116] for instance, developed a bi-domain FE model that discriminates between the intracellular structures and extracellular matrices of musculotendons. Muscle fibres and connective tissues were discretised as separate meshes that occupied the same space and linked elastically. This approach allowed them to model the interaction between myofibrils and the extracellular matrix to account for mechanical forces that are transferred between these two domains. The study of [85] also developed FE models for mechanical strain distribution and explored the effects of aponeurosis geometry on elongation during tensile loads. The results of the study introduced a new hypothesis to test how significant the width of aponeuroses is when determining the sensitivity of skeletal muscle to straining, where the model suggested a correlation between narrow aponeuroses and high localised mechanical strains. Furthermore, the seminal work of [32] revealed that variations in length and curvature of fascicles are the primary factors that contribute to non-uniform mechanical strains. The above given references serve as a testament to the non-linear complexity inherent in biological systems.

2.4.6 Sprain

Unlike strain injuries that affects muscles or tendons, a sprain is defined in [28] as a joint injury that leads to partial tearing or stretching of supporting ligaments. One example of a popular sprain injury is the sprained ankle. This is due to the energy consumption of the ankle, which according to [54] accounts for approximately 51% during walk-cycles. Ankle sprain occurs when one or more surrounding ligaments in the ankle get (partially) torn. According to [10], primary causes can be twisting, turning, and rolling of the foot beyond its normal range of motion. In biomechanics, studies have been carried out by [112] and [111] that examined the influence of foot-positioning and joint-flexibility and compliance on ankle sprain occurrences. Results from the simulations carried out by [112] suggests that touching down the foot in plantar flexion during gait cycles increases the susceptibility of ankle sprains for patients with an ankle sprain history. [111] concluded that at least for side-shuffle movements, an increase in mechanical laxity does not automatically signify an increase in ankle sprain injuries.

2.4.7 Dislocation

Similarly to sprains, [28] defines a dislocation as the displacement of bone ends at the joint that result in abnormal stretching of the ligaments around the joint. In some cases the dislocation causes severe sprains and even complete ligament separation. Broken ligaments make a joint unstable and could, over a period of time, result in degradation of the articular cartilage or even osteoarthritis.

2.4.8 Fracture

Following the description in [28], a break in the continuity of bone that may result in a partial or complete disruption of bone defines a fracture. Fractures can be classified as open or closed where the former classifies an initial injury where bone ends have produced an open wound at or near the fracture site. The latter classifies a fracture where the bone is broken into smaller fragments but did not have any outer skin penetration, e.g. a direct

hit on the proximal end of the ulna (at the elbow) where broken pieces get scattered within the surrounding tissue.

Bones of the skeleton are susceptible to fractures. This is due to the inherent property of mammalian bone as being both brittle and ductile with time-dependent behaviour. The material properties of bone consist of both collagen and hydroxyapatite as is mentioned in section 2.1.1. [90] states that bone is one of the most frequently investigated materials in which finite element analysis (FEA) was deemed as a useful tool. [58] highlights the long history of FEA in bone research that started since 1972. Since then, as conventional computing power increased due to Moore's law, more complex FE models have been developed.

The structure of bone, heterogenous, anisotropic, and has several hierarchies. The survey of [90] outlines different modelling strategies that were introduced for both macro and micro levels to investigate clinical as well as fundamental problems in bone mechanics. [105] for instance assessed micro-structural FE models (μFE) for the prediction of load failures. A contour-plot of the distal radius containing over 18.2 million brick elements that are 80 μm^3 in volume is shown in Figure 23a. Other FE models such as ones used in work of [47] and [40] investigated fracture injuries at the angle of the mandible[8]. Fractures of the angle of the mandible are considered one of the most common and problematic regions of all facial fractures because of the high frequency of complications and the difficulty of getting surgical access to the affected area according to [108] and [52]. Research of [47] carried out the first biomechanical FEA of mandibular angle fractures. [63] used FE models to evaluate and confirm with clinical observations which angle-fixation-approach gives the best outcome for patients.

While previously mentioned works focused on the management of mandibular fractures, [40] focused instead on mandibular angle fractures caused by high speed projectiles such as bullets. They developed a combined hexahedral-tetrahedral FE model of the mandible of a pig to simulate ballistic impact and mandible penetration, visible in Figure 23b. The results showed no statistical differences between the FE simulation and an experimental study with respect to the residual velocity, the transferred energy from the bullet to the mandible, and also the mean surface area of the entrance wound. However, they did find significant differences between the mean surface area of the exit wound, which was larger in the FE simulation. One possible reason that the authors attribute to this discrepancy is the homogenous and isotropic assumption of their FE model.

In the field of computer graphics and computational geometry, the innovative work of [80] simulated both linear brittle (elastic) and ductile (plastic) deformation before fracturing, hence effectively splitting total strain into its elastic and plastic constituents. Figure 25a shows one result comparing simulation versus a real experiment with clay. The algorithm uses the *von Mises* yield criterion to decide when plastic deformation should commence. Although the model preserves volume by excluding dilation effects, it excludes time-dependent phenomena such as creep, stress relaxation, and fatigue due to applying solely linear constitutive relations. More recently, [53] used the level-set method for ductile fracture, removing the need for remeshing of polygonal objects. However, with this shape-based approach, they cannot simulate the physical phenomenon of crack tips. In addition, collision management is not granular enough to prevent complete separation. Figure 24 shows one result with projectile penetrating a block of jello. [83] presented a framework for elastic and plastic deformation using adaptive surface-elements instead of FEM. Although flexible in handling wide range of material properties, the large time-steps required are not suited for the simulation of brittle materials. Furthermore, they adopt

[8]The mandible (commonly known as the jawbone) forms the lower jaw that holds the lower teeth into place. The angle of the mandible lies at a junction between the lower border and the posterior border of the ramus of the mandible.

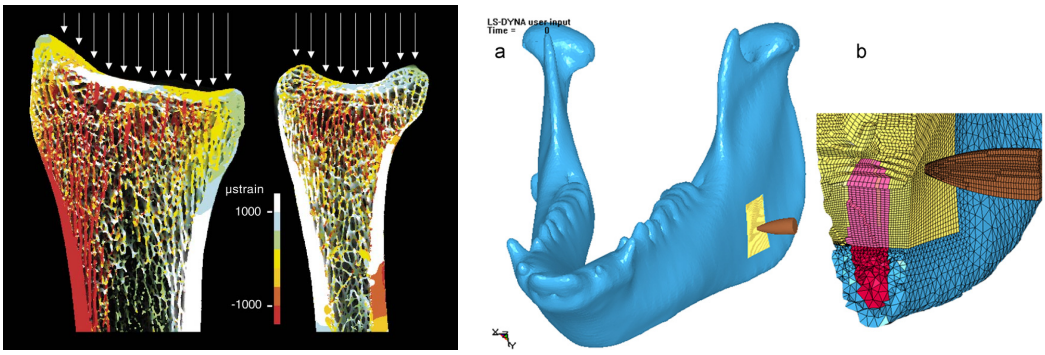

(a) **(b)**

Figure 23: **(a)** - Image taken from [105] showing a contour plot of a μFE model with the computed result of a principal strain distribution in the distal radius for a load of 1.000N. The 3D μFE model contains over 12.8 million eight-node brick elements that are 80 μm^3 in volume. Yellow - red colours visualise compressive strain while blue - green colours visualise tensile strain (2006). **(b)** - Work from [40] showing the combined FE model (left) and a close-up (right) of the redefined hexahedral mesh (each consisting of eight-node brick elements) for the impact region with the bullet contact-point (2010).

a penalty-scheme for collisions that unfortunately does not guarantee collision-free self-intersections. [82] focused on the real-time aspect of fractures and developed a robust framework based on linear co-rotational FEM. This to factor out the rotational dependency inherent in linear analysis similar to [75] and [46]. The actual deformation on a mesh is executed on the GPU via shader programs. Hereto, vertices of a breakable object are not stored in usual Cartesian coordinates, but instead are stored relatively via barycentric coordinates, where each set of weights defines one vertex-position of the 3D object. Due to the real-time constraint, the fracture algorithm excludes remeshing, which is essential to visualise details along the boundaries of the split. To circumvent this limitation, they developed the concept of *splinters*, shown in Figure 25b, which are geometries smaller than the course tetrahedral mesh. Splinters are defined manually and are rendered as embedded surfaces. The centroid of each splinter is used to decide in which tetrahedron the splinter belongs to during the fracturing process. Finally, more recent work from [36] looked at the simulation of fractures for thin plates. They improved upon the realism through the inclusion of the following three key features. First, the material was modelled with multiple layers to account for separation effects of thin layers. Next, for the remeshing scheme they used Delaunay triangulation to generate detailed fracture animations. Lastly, they applied a stress relaxation method to prevent objects from fracturing into small pieces and unwontedly getting separated from the mesh.

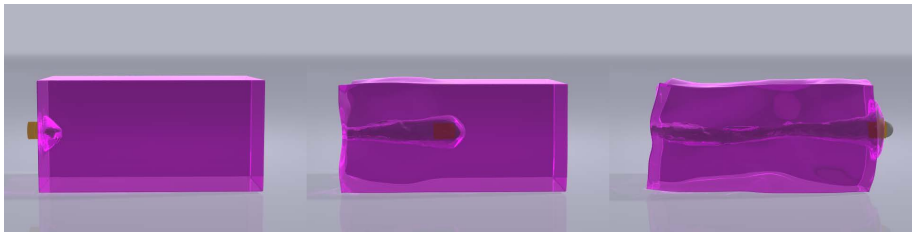

Figure 24: Result of [53] showing the permanent cavity, shaped by the level-set function for a passed bullet through jello-like material (2013).

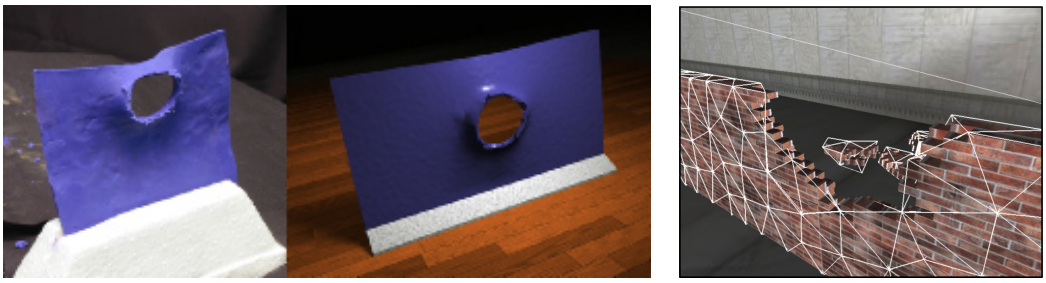

(a) **(b)**

Figure 25: (a) - Work from [80] showing a comparison between two tests of clay being penetrated by a spherical projectile. The left image is a real photograph, while the right image is the simulated result (2002). **(b)** - Work from [82] showing a higher resolution mesh embedded in a real-time tetrahedral FE model. The high resolution mesh is also divided into discrete units known as splinters to aid in the realism of the splitting procedure while fracturing (2009).

3 Discussion and Conclusion

This section starts with a brief description on the master project in brief coupled with potential problems that might arise, and ends with some concluding remarks.

3.1 The Master Project

The first objective of the master project is to simulate musculoskeletal injuries with the aid of a validated model that is suitable for real-time use. This objective can be further divided into the following three sub-tasks:

- Create and attach a musculoskeletal model unto a 3D human mesh that allows injuries to be possible.
- Perform real-time simulations of musculoskeletal injuries and validate the injuries.
- Use the injury simulation to assess the inflicted damage and (optionally) modify the animation to adapt the behaviour of the character to its new situation.

In addition, the animation group at Utrecht University is developing an animation platform codenamed RAGE, which stands for Real-Time Animation Game Engine. This master project will be implemented within that platform. Development will be mostly done in the programming language C++ with Microsoft® Visual Studio® 2010. Currently, RAGE uses the Ogre3D Graphics platform for rendering [4]. For the GUI, Python scripts will be created in order to interact with several parameters in real-time. The current pipeline for character animation in RAGE uses skeleton-subspace deformation (SSD) with key-frame interpolation. The animation data is supplied by motion-capture sessions at Utrecht University provided in the Biovision Hierarchy (BVH) format. Due to the use of pre-recorded motion, the musculoskeletal model will be build on top of the already existing key-frame system. Therefore, forward-dynamics (or dynamic optimisation) is not a requirement for the project. However, inverse dynamics (static optimisation) could be useful if physics-based techniques are to be implemented.

Another important aspect to consider for model development is the type of injury that will be simulated in the project. Each type of injury would require a different approach. For instance, the modelling of sprain and strain injuries could suffice with an embedded biomechanical model coupled with inverse dynamics to simulate over-exertion of musculotendons and ligaments. Skin related injuries would probably use more complex soft-deformation techniques that simulate the non-linear viscoelastic behaviour of

human skin, or perhaps approximations with simpler shape functions that can visualise a deformed patch of surface. Severe injuries usually constitute a deeper penetration-depth within the inner structures of the human body, thereby most likely requiring non-linear approximation of continuum models. For FEM, the amount of suspected deformation would play a role in whether to opt for an implicit or explicit model. Explicit FEM supports larger deformation and shorter time-steps, but is in general more computationally expensive. In addition, injuries such as bone fractures and amputations that require a sound computational model to account for large deformations and fragmentation would also require a robust collision management system when dealing with more than one type of tissue in the damaged region.

Lastly, the real-time constraint imposed on the project brings to light the discussion between accuracy versus real-time performance. The human body is inherently complex, and complexity requires extra computations, which slow the simulation down. In addition, the pursuit for real-time performance can introduce a caveat regarding the flexibility of a framework. A flexible framework is one that is able to scale easily without requiring much adaptations to the proposed ideas and techniques, or limitations on generality due to specific technical optimisations. Therefore, developing a general method that is real-time and able to adapt its resolution is no easy feat. On the other hand, accurate and complex methods that are both realistic and flexible, such as FEM, are steadily converging in the real-time domain as time goes by.

3.2 Final Remarks

The body of literature reviewed here, part of the master project entitled *Real-Time Musculoskeletal Model for Injury Simulation on 3D Human Characters*, covered several fields in order to bridge potential knowledge-gaps. A problem by itself that requires a multi-disciplinary background to fully understand the science. The broad range of work that was covered serves as a testament to the complexity inherent in the biology and physics of the human body. From biomechanical models embedded into inverse-dynamics pipelines to more accurate simulations that create movements with forward dynamics, the increase in computing power coinciding with the higher accuracy of models will ultimately lead to more beneficial and practical applications that make use of digital human characters.

References

[1] Aaam's abbreviated injury scale, 2005. URL `http://www.aaam1.org/ais/`.

[2] Injury severity score, March 2007. URL `http://www.trauma.org/index.php/main/article/383/`.

[3] File:caput femoris cortex medulla.jpg - wikipedia, the free encyclopedia, 2008. URL `http://en.wikipedia.org/wiki/File:Caput_femoris_cortex_medulla.jpg`.

[4] Ogre – open source 3d graphics engine, December 2009. URL `http://www.ogre3d.org/`.

[5] File:hyperelastic.svg - wikipedia, the free encyclopedia, 2010. URL `http://en.wikipedia.org/wiki/File:Hyperelastic.svg`.

[6] Better engine: Experience the physical battlefield in the all-new frostbite 2 game engine, 2012. URL `http://www.battlefield.com/battlefield3/1/frostbite2`.

[7] Bvi - body volume index, 2012. URL `http://www.bodyvolume.com/`.

[8] Crytek — mycryengine, 2012. URL http://mycryengine.com/index.php?conid=17.

[9] morphology (biology) – encyclopedia britannica, 2012. URL http://www.britannica.com/EBchecked/topic/392797/morphology.

[10] Sprained ankle-orthoinfo - aaos, September 2012. URL http://orthoinfo.aaos.org/topic.cfm?topic=A00150.

[11] File:bertazzo s - sem deproteined trabecular - wistar rat - x100.tif - wikipedia, the free encyclopedia, 2012. URL http://en.wikipedia.org/wiki/File:Bertazzo_S_-_SEM_deproteined_trabecular_-_wistar_rat_-_x100.tif.

[12] 3d animation modeling software, 2012. URL http://www.unrealengine.com/features/animation/.

[13] Dictionary of cancer terms, 2012. URL http://www.cancer.gov/Common/PopUps/popDefinition.aspx?id=45882.

[14] Anatomical terms of location — wikipedia, the free encyclopedia, 2012. URL http://en.wikipedia.org/w/index.php?title=Anatomical_terms_of_location&oldid=476530117.

[15] 2740 connective tissues, August 2013. URL http://www.unomaha.edu/hpa/2740cartilagebone.html.

[16] 2740 connective tissues, August 2013. URL http://www.unomaha.edu/hpa/2740connectivetissue.html.

[17] anatomyexpert - structure detail, August 2013. URL http://www.anatomyexpert.com/structure_detail/17270/1614/.

[18] File:joint.svg - wikimedia commons, July 2013. URL http://commons.wikimedia.org/wiki/File:Joint.svg.

[19] File:right hand skeleton.gif - wikimedia commons, July 2013. URL http://commons.wikimedia.org/wiki/File:Right_hand_skeleton.gif.

[20] Karim Abdel-Malek, Jingzhou Yang, Timothy Marler, Steven Beck, Anith Mathai, Xianlian Zhou, Amos Patrick, and Jasbir Arora. Towards a new generation of virtual humans. *International Journal of Human Factors Modelling and Simulation*, 1:2–39, January 2006.

[21] Bilal A. Ahmed, Michael E. Matheny, Phillip L. Rice, John R. Clarke, and Omolola I. Ogunyemi. A comparison of methods for assessing penetrating trauma on retrospective multi-center data. *Journal of Biomedical Informatics*, 42(2): 308–316, 2009. ISSN 1532-0464. doi: 10.1016/j.jbi.2008.09.002. URL http://www.sciencedirect.com/science/article/pii/S1532046408001238.

[22] Irene Albrecht, Jörg Haber, and Hans-Peter Seidel. Construction and animation of anatomically based human hand models. In *Proceedings of the 2003 ACM SIGGRAPH/Eurographics symposium on Computer animation*, SCA '03, pages 98–109, Aire-la-Ville, Switzerland, Switzerland, 2003. Eurographics Association. ISBN 1-58113-659-5. URL http://dl.acm.org/citation.cfm?id=846276.846290.

[23] Alessia Amelio and Clara Pizzuti. Skin lesion image segmentation using a color genetic algorithm. In *Proceeding of the fifteenth annual conference companion on Genetic and evolutionary computation conference companion*, GECCO '13

Companion, pages 1471–1478, New York, NY, USA, 2013. ACM. ISBN 978-1-4503-1964-5. doi: 10.1145/2464576.2466810. URL http://doi.acm.org/10.1145/2464576.2466810.

[24] Anthony Aquilio, Jeremy Brooks, Ying Zhu, and G. Owen. Real-time gpu-based simulation of dynamic terrain. In George Bebis, Richard Boyle, Bahram Parvin, Darko Koracin, Paolo Remagnino, Ara Nefian, Gopi Meenakshisundaram, Valerio Pascucci, Jiri Zara, Jose Molineros, Holger Theisel, and Tom Malzbender, editors, *Advances in Visual Computing*, volume 4291 of *Lecture Notes in Computer Science*, pages 891–900. Springer Berlin / Heidelberg, 2006.

[25] A. Aubel and D. Thalmann. Interactive modeling of the human musculature. In *Computer Animation, 2001. The Fourteenth Conference on Computer Animation. Proceedings*, pages 167–255, 2001. doi: 10.1109/CA.2001.982390.

[26] Richard Barnes and Asad Rahim. The body volume index: new imaging technology for body measurement. *Hospital Imaging and Radiology Europe*, 4(3), October 2009.

[27] F. Barthelat. Biomimetics for next generation materials. *Royal Society of London Philosophical Transactions Series A*, 365:2907–2919, December 2007.

[28] Field Medical Training Battalion. Manage musculoskeletal injuries. Camp Lejeune, North Carolina, February 2009.

[29] Y. Berranen, M. Hayashibe, B. Gilles, and D. Guiraud. 3d volumetric muscle modeling for real-time deformation analysis with fem. In *Engineering in Medicine and Biology Society (EMBC), 2012 Annual International Conference of the IEEE*, pages 4863–4866, 2012. doi: 10.1109/EMBC.2012.6347083.

[30] D. Bielser, P. Glardon, M. Teschner, and M. Gross. A state machine for real-time cutting of tetrahedral meshes. *Graphical Models*, 66(6):398 – 417, 2004. ISSN 1524-0703. doi: http://dx.doi.org/10.1016/j.gmod.2004.05.009. URL http://www.sciencedirect.com/science/article/pii/S1524070304000529.

[31] Daniel Bielser, Volker A. Maiwald, and Markus H. Gross. Interactive cuts through 3-dimensional soft tissue. *Computer Graphics Forum*, 18(3):31–38, 1999. ISSN 1467-8659. doi: 10.1111/1467-8659.00325. URL http://dx.doi.org/10.1111/1467-8659.00325.

[32] Silvia S. Blemker, Peter M. Pinsky, and Scott L. Delp. A 3d model of muscle reveals the causes of nonuniform strains in the biceps brachii. *Journal of Biomechanics*, 38(4):657 – 665, 2005. ISSN 0021-9290. doi: http://dx.doi.org/10.1016/j.jbiomech.2004.04.009. URL http://www.sciencedirect.com/science/article/pii/S0021929004001940.

[33] SilviaS. Blemker and ScottL. Delp. Three-dimensional representation of complex muscle architectures and geometries. *Annals of Biomedical Engineering*, 33(5): 661–673, 2005. ISSN 0090-6964. doi: 10.1007/s10439-005-1433-7. URL http://dx.doi.org/10.1007/s10439-005-1433-7.

[34] Robert Bridson, Ronald Fedkiw, and John Anderson. Robust treatment of collisions, contact and friction for cloth animation. In *Proceedings of the 29th annual conference on Computer graphics and interactive techniques*, SIGGRAPH '02, pages 594–603, New York, NY, USA, 2002. ACM. ISBN 1-58113-521-1. doi: 10.1145/566570.566623. URL http://doi.acm.org/10.1145/566570.566623.

[35] Morten Bro-Nielsen and Stephane Cotin. Real-time volumetric deformable models for surgery simulation using finite elements and condensation. *Computer Graphics Forum*, 15(3):57–66, 1996. ISSN 1467-8659. doi: 10.1111/1467-8659.1530057. URL http://dx.doi.org/10.1111/1467-8659.1530057.

[36] Oleksiy Busaryev, Tamal K. Dey, and Huamin Wang. Adaptive fracture simulation of multi-layered thin plates. *ACM Trans. Graph.*, 32(4):52:1–52:6, July 2013. ISSN 0730-0301. doi: 10.1145/2461912.2461920. URL http://doi.acm.org/10.1145/2461912.2461920.

[37] J.R. Cameron, J.G. Skofronick, and R.M. Grant. *Physics of the Body*. Medical Physics Series. Medical Physics Publishing Corporation, 1999. ISBN 9780944838914. URL http://books.google.nl/books?id=ro59QgAACAAJ.

[38] J. E. Chadwick, D. R. Haumann, and R. E. Parent. Layered construction for deformable animated characters. In *Proceedings of the 16th annual conference on Computer graphics and interactive techniques*, SIGGRAPH '89, pages 243–252, New York, NY, USA, 1989. ACM. ISBN 0-89791-312-4. doi: 10.1145/74333.74358. URL http://doi.acm.org/10.1145/74333.74358.

[39] David T. Chen and David Zeltzer. Pump it up: computer animation of a biomechanically based model of muscle using the finite element method. In *Proceedings of the 19th annual conference on Computer graphics and interactive techniques*, SIGGRAPH '92, pages 89–98, New York, NY, USA, 1992. ACM. ISBN 0-89791-479-1. doi: 10.1145/133994.134016. URL http://doi.acm.org/10.1145/133994.134016.

[40] Yubin Chen, Yingyun Miao, Chuan Xu, Gang Zhang, Tao Lei, and Yinghui Tan. Wound ballistics of the pig mandibular angle: A preliminary finite element analysis and experimental study. *Journal of Biomechanics*, 43:1131–1137, 2010.

[41] Stephane Cotin, H. Delingette, and N. Ayache. Real-time elastic deformations of soft tissues for surgery simulation. *Visualization and Computer Graphics, IEEE Transactions on*, 5(1):62–73, 1999. ISSN 1077-2626. doi: 10.1109/2945.764872.

[42] Stphane Cotin, Herv Delingette, and Nicholas Ayache. A hybrid elastic model for real-time cutting, deformations, and force feedback for surgery training and simulation. *The Visual Computer*, 16(8):437–452, 2000. ISSN 0178-2789. doi: 10.1007/PL00007215. URL http://dx.doi.org/10.1007/PL00007215.

[43] JOHN Dolbow and T Belytschko. A finite element method for crack growth without remeshing. *Int. J. Numer. Meth. Engng*, 46:131–150, 1999.

[44] LeAnn M. Dourte, Andrew F. Kuntz, and Louis J. Soslowsky. Twenty-five years of tendon and ligament research. *Journal of Orthopaedic Research*, 26(10):1297–1305, 2008. ISSN 1554-527X. doi: 10.1002/jor.20646. URL http://dx.doi.org/10.1002/jor.20646.

[45] Richard L. Drake, Wayne Vogl, and Adam W.M. Mitchell. *Gray's Anatomy for Students*. Churchill Livingstone, 2nd edition, 2009.

[46] O. Etzmuss, M. Keckeisen, and W. Strasser. A fast finite element solution for cloth modelling. In *Computer Graphics and Applications, 2003. Proceedings. 11th Pacific Conference on*, pages 244–251, 2003. doi: 10.1109/PCCGA.2003.1238266.

[47] José R. Fernández, M. Gallasb, M. Burgueraa, and J.M. Viañoa. A three-dimensional numerical simulation of mandible fracture a three-dimensional numerical simulation of mandible fracture reduction with screwed miniplates. *Journal of Biomechanics*, 36:329–337, 2003.

[48] W.A. Fetter. A progression of human figures simulated by computer graphics. *IEEE Computer Graphics and Applications*, 2:9–13, November 1982.

[49] F. Ganovelli and C. O'Sullivan. Animating cuts with on-the-fly re-meshing. *EUROGRAPHICS 2001: Short presentations*, 2001.

[50] Fabio Ganovelli, Paolo Cignoni, Claudio Montani, and Roberto Scopigno. A multiresolution model for soft objects supporting interactive cuts and lacerations. *Computer Graphics Forum*, 19(3):271–281, 2000. ISSN 1467-8659. doi: 10.1111/1467-8659.00419. URL `http://dx.doi.org/10.1111/1467-8659.00419`.

[51] L.J. Gibson and M.F. Ashby. *Cellular Solids: Structure and Properties*. Cambridge Solid State Science Series. Cambridge University Press, 1999. ISBN 9780521499118. URL `http://books.google.nl/books?id=IySUr5sn4N8C`.

[52] R.H. Haug, J. Prather, and A.T. Indresano. An epidemiologic survey of facial fractures and concomitant injuries. *Journal of Oral and Maxillofacial Surgery*, 48: 926–932, 1990.

[53] Jan Hegemann, Chenfanfu Jiang, Craig Schroeder, and Joseph M. Teran. A level set method for ductile fracture. In *Proceedings of the 12th ACM SIGGRAPH/Eurographics Symposium on Computer Animation*, SCA '13, pages 193–201, New York, NY, USA, 2013. ACM. ISBN 978-1-4503-2132-7. doi: 10.1145/2485895.2485908. URL `http://doi.acm.org/10.1145/2485895.2485908`.

[54] Aaron Hertzmann, Carol O'Sullivan, and Ken Perlin. Realistic human body movement for emotional expressiveness. In *ACM SIGGRAPH 2009 Courses*, SIGGRAPH '09, pages 20:1–20:27, New York, NY, USA, 2009. ACM. doi: 10.1145/1667239.1667259. URL `http://doi.acm.org/10.1145/1667239.1667259`.

[55] S B Heymsfield, S Lichtman, R N Baumgartner, J Wang, Y Kamen, A Aliprantis, and R N Pierson. Body composition of humans: comparison of two improved four-compartment models that differ in expense, technical complexity, and radiation exposure. *The American Journal of Clinical Nutrition*, 52(1):52–8, 1990. URL `http://ajcn.nutrition.org/content/52/1/52.abstract`.

[56] Gentaro Hirota, Susan Fisher, Chris Lee, H Fuchs, et al. An implicit finite element method for elastic solids in contact. In *Computer Animation, 2001. The Fourteenth Conference on Computer Animation. Proceedings*, pages 136–254. IEEE, 2001.

[57] James A. Hodgdon and Karl Friedl. Development of the dod body composition estimation equations. *DITC Online: Information for the Defense Community*, September 1999.

[58] R Huiskes and EYS Chao. A survey of finite element analysis in orthopedic biomechanics: the first decade. *Journal of Biomechanics*, 16(6):385–409, 1983.

[59] Andrew F Huxley. Muscle structure and theories of contraction. *Prog. Biophys. Biophys. Chem*, 7:255–318, 1957.

[60] Andrew F Huxley and Ro M Simmons. Proposed mechanism of force generation in striated muscle. *Nature*, 233:533–538, 1971.

[61] Neha Jain. Finite element approach to radial heat flow in human dermal tissues. In VinuV Das, R. Vijayakumar, NarayanC. Debnath, Janahanlal Stephen, Natarajan Meghanathan, Suresh Sankaranarayanan, P.M. Thankachan, FordLumban Gaol, and Nessy Thankachan, editors, *Information Processing and Management*, volume 70 of *Communications in Computer and Information Science*, pages 369–375. Springer Berlin Heidelberg, 2010. ISBN 978-3-642-12213-2. doi: 10.1007/978-3-642-12214-9_59. URL http://dx.doi.org/10.1007/978-3-642-12214-9_59.

[62] E. Keeve, S. Girod, P. Pfeifle, and B. Girod. Anatomy-based facial tissue modeling using the finite element method. In *Visualization '96. Proceedings.*, pages 21–28, 1996. doi: 10.1109/VISUAL.1996.567595.

[63] J. Kimsal, B. Baack, L. Candelaria, T. Khraishi, and S. Lovald. Biomechanical analysis of mandibular angle fractures. *Journal of Oral and Maxillofacial Surgery*, 69:3010–3014, 2011.

[64] Koji Komatsu. Human skin model capable of natural shape variation. *The Visual Computer*, 3(5):265–271, 1988. ISSN 0178-2789. doi: 10.1007/BF01914861. URL http://dx.doi.org/10.1007/BF01914861.

[65] R.J. Lapeer, P.D. Gasson, and V. Karri. Simulating plastic surgery: From human skin tensile tests, through hyperelastic finite element models to real-time haptics. *Progress in Biophysics and Molecular Biology*, 103(2-3):208 – 216, 2010.

[66] Dongwoon Lee, MICHAEL GLUECK, AZAM KHAN, EUGENE FIUME, and KEN JACKSON. A survey of modeling and simulation of skeletal muscle. *ACM Transactions on Graphics*, 28(4), 2010.

[67] Keng Siang Lee and Golam Ashraf. Simplified muscle dynamics for appealing real-time skin deformation. *International Conference on Computer Graphics and Virtual Reality*, 2007.

[68] Yuencheng Lee, Demetri Terzopoulos, and Keith Waters. Realistic modeling for facial animation. In *Proceedings of the 22nd annual conference on Computer graphics and Interactive techniques*, SIGGRAPH '95, pages 55–62, New York, NY, USA, 1995. ACM. ISBN 0-89791-701-4. doi: 10.1145/218380.218407. URL http://doi.acm.org/10.1145/218380.218407.

[69] R. Lemos, M. Epstein, W. Herzog, and B. Wyvill. Realistic skeletal muscle deformation using finite element analysis. In *Computer Graphics and Image Processing, 2001 Proceedings of XIV Brazilian Symposium on*, pages 192–199, 2001. doi: 10.1109/SIBGRAPI.2001.963055.

[70] J. P. Lewis, Matt Cordner, and Nickson Fong. Pose space deformation: a unified approach to shape interpolation and skeleton-driven deformation. In *Proceedings of the 27th annual conference on Computer graphics and interactive techniques*, SIGGRAPH '00, pages 165–172, New York, NY, USA, 2000. ACM Press/Addison-Wesley Publishing Co. ISBN 1-58113-208-5. doi: 10.1145/344779.344862. URL http://dx.doi.org/10.1145/344779.344862.

[71] Alex Lindblad and George Turkiyyah. A physically-based framework for real-time haptic cutting and interaction with 3d continuum models. In *Proceedings of the 2007 ACM symposium on Solid and physical modeling*, SPM '07, pages 421–429, New York, NY, USA, 2007. ACM. ISBN 978-1-59593-666-0. doi: 10.1145/1236246.1236307. URL http://doi.acm.org/10.1145/1236246.1236307.

[72] Elaine N. Marieb and Katja Hoehn. *Human Anatomy and Physiology*. Benjamin Cummings, 7th edition, January 2006.

[73] Karol Miller, Grand Joldes, Dane Lance, and Adam Wittek. Total langrangian explicit dynamics finite element algorithm for computing soft tissue deformation. *Communications in Numerical Methods in Engineering*, 23:121–134, August 2006.

[74] Neil Molino, Zhaosheng Bao, and Ron Fedkiw. A virtual node algorithm for changing mesh topology during simulation. In *ACM SIGGRAPH 2004 Papers*, SIGGRAPH '04, pages 385–392, New York, NY, USA, 2004. ACM. doi: 10.1145/1186562.1015734. URL `http://doi.acm.org/10.1145/1186562.1015734`.

[75] Matthias Müller and Markus Gross. Interactive virtual materials. In *Proceedings of Graphics Interface 2004*, GI '04, pages 239–246, School of Computer Science, University of Waterloo, Waterloo, Ontario, Canada, 2004. Canadian Human-Computer Communications Society. ISBN 1-56881-227-2. URL `http://dl.acm.org/citation.cfm?id=1006058.1006087`.

[76] L.P. Nedel and D. Thalmann. Real time muscle deformations using mass-spring systems. In *Computer Graphics International, 1998. Proceedings*, pages 156–165, 1998. doi: 10.1109/CGI.1998.694263.

[77] Victor Ng-Thow-Hing. *Anatomically-based Models for Physical and Geometric Reconstruction of Humans and Other Animals*. PhD thesis, University of Toronto, 2001.

[78] Han-Wen Nienhuys and A Frank van der Stappen. Combining finite element deformation with cutting for surgery simulations. In *EUROGRAPHICS 2000: Short Presentations*. Citeseer, 2000.

[79] Margareta Nordin and Victor H. Frankel. *Basic Biomechanics of the Musculoskeletal System*. Wolters Kluwer Health, 4th edition, 2012.

[80] James F. O'Brien, Adam W. Bargteil, and Jessica K. Hodgins. Graphical modeling and animation of ductile fracture. In *Proceedings of the 29th annual conference on Computer graphics and interactive techniques*, SIGGRAPH '02, pages 291–294, New York, NY, USA, 2002. ACM. ISBN 1-58113-521-1. doi: 10.1145/566570.566579. URL `http://doi.acm.org/10.1145/566570.566579`.

[81] Omolola Ogunyemi. Methods for reasoning from geometry about anatomic structures injured by penetrating trauma. *Journal of Biomedical Informatics*, 39 (4):389–400, 2006. ISSN 1532-0464. doi: 10.1016/j.jbi.2005.10.005. URL `http://www.sciencedirect.com/science/article/pii/S1532046405001073`.

[82] Eric G. Parker and James F. O'Brien. Real-time deformation and fracture in a game environment. In *Proceedings of the 2009 ACM SIGGRAPH/Eurographics Symposium on Computer Animation*, SCA '09, pages 165–175, New York, NY, USA, 2009. ACM. ISBN 978-1-60558-610-6. doi: 10.1145/1599470.1599492. URL `http://doi.acm.org/10.1145/1599470.1599492`.

[83] Mark Pauly, Richard Keiser, Bart Adams, Philip Dutré, Markus Gross, and Leonidas J. Guibas. Meshless animation of fracturing solids. In *ACM SIGGRAPH 2005 Papers*, SIGGRAPH '05, pages 957–964, New York, NY, USA, 2005. ACM. doi: 10.1145/1186822.1073296. URL `http://doi.acm.org/10.1145/1186822.1073296`.

[84] Guillaume Picinbono, Jean-Christophe Lombardo, Herv Delingette, and Nicholas Ayache. Improving realism of a surgery simulator: linear anisotropic elasticity, complex interactions and force extrapolation. *The Journal of Visualization and Computer Animation*, 13(3):147–167, 2002. ISSN 1099-1778. doi: 10.1002/vis.257. URL http://dx.doi.org/10.1002/vis.257.

[85] Michael R. Rehorn and Silvia S. Blemker. The effects of aponeurosis geometry on strain injury susceptibility explored with a 3d muscle model. *Journal of Biomechanics*, 43(13):2574 – 2581, 2010. ISSN 0021-9290. doi: http://dx.doi.org/10.1016/j.jbiomech.2010.05.011. URL http://www.sciencedirect.com/science/article/pii/S0021929010002812.

[86] C.T.F. Ross. *Mechanics of solids*. Ellis Horwood series in engineering science. Horwood Pub., 1999. ISBN 9781898563679. URL http://books.google.nl/books?id=H_5zV2twBtwC.

[87] Cornelius Rosse and Jr Mejino, JoséL.V. The foundational model of anatomy ontology. In Albert Burger, Duncan Davidson, and Richard Baldock, editors, *Anatomy Ontologies for Bioinformatics*, volume 6 of *Computational Biology*, pages 59–117. Springer London, 2008. ISBN 978-1-84628-884-5. doi: 10.1007/978-1-84628-885-2_4. URL http://dx.doi.org/10.1007/978-1-84628-885-2_4.

[88] S.H. Roth, Markus H. Gross, Silvio Turello, and Friedrich R. Carls. A bernstein-bézier based approach to soft tissue simulation. *Computer Graphics Forum*, 17(3):285–294, 1998. ISSN 1467-8659. doi: 10.1111/1467-8659.00275. URL http://dx.doi.org/10.1111/1467-8659.00275.

[89] Daniel L. Rubin, Olivier Dameron, Yasser Bashir, David Grossman, Parvati Dev, and Mark A. Musen. Using ontologies linked with geometric models to reason about penetrating injuries. *Artificial Intelligence in Medicine*, 37(3):167–176, 2006. ISSN 0933-3657. doi: 10.1016/j.artmed.2006.03.006. URL http://www.sciencedirect.com/science/article/pii/S0933365706000522.

[90] D. Ruffoni and G.H. van Lenthe. Finite element analysis in bone research: A computational method relating structure to mechanical function. In Paul Ducheyne, editor, *Comprehensive Biomaterials*, pages 91 – 111. Elsevier, Oxford, 2011. ISBN 978-0-08-055294-1. doi: 10.1016/B978-0-08-055294-1.00093-3. URL http://www.sciencedirect.com/science/article/pii/B9780080552941000933.

[91] Ferdi Scheepers, Richard E. Parent, Wayne E. Carlson, and Stephen F. May. Anatomy-based modeling of the human musculature. In *Proceedings of the 24th annual conference on Computer graphics and interactive techniques*, SIGGRAPH '97, pages 163–172, New York, NY, USA, 1997. ACM Press/Addison-Wesley Publishing Co. ISBN 0-89791-896-7. doi: 10.1145/258734.258827. URL http://dx.doi.org/10.1145/258734.258827.

[92] S. Schein and G. Elber. Discontinuous free form deformations. In *Computer Graphics and Applications, 2004. PG 2004. Proceedings. 12th Pacific Conference on*, pages 227–236, 2004. doi: 10.1109/PCCGA.2004.1348353.

[93] Guy Sela, Jacob Subag, Alex Lindblad, Dan Albocher, Sagi Schein, and Gershon Elber. Real-time haptic incision simulation using fem-based discontinuous free-form deformation. *Computer-Aided Design*, 39(8):685 – 693, 2007. ISSN 0010-4485. doi: http://dx.doi.org/10.1016/j.cad.2007.05.011. URL http://www.sciencedirect.com/science/article/pii/S0010448507001145.

[94] Hyewon Seo and Nadia Magnenat-Thalmann. An example-based approach to human body manipulation. *Graph. Models*, 66(1):1–23, January 2004. ISSN 1524-0703. doi: 10.1016/j.gmod.2003.07.004. URL http://dx.doi.org/10.1016/j.gmod.2003.07.004.

[95] J.M. Spivak and N.Y.) Hospital for Joint Diseases Orthopaedic Institute (New York. *Orthopaedics: A Study Guide*. McGraw-Hill, 1999. ISBN 9780070603554. URL http://books.google.nl/books?id=atVsAAAAMAAJ.

[96] Denis Steinemann, Miguel A. Otaduy, and Markus Gross. Fast arbitrary splitting of deforming objects. In *Proceedings of the 2006 ACM SIGGRAPH/Eurographics symposium on Computer animation*, SCA '06, pages 63–72, Aire-la-Ville, Switzerland, Switzerland, 2006. Eurographics Association. ISBN 3-905673-34-7. URL http://dl.acm.org/citation.cfm?id=1218064.1218073.

[97] G Szkely, Ch Brechbhler, R Hutter, A Rhomberg, N Ironmonger, and P Schmid. Modelling of soft tissue deformation for laparoscopic surgery simulation. *Medical Image Analysis*, 4(1):57 – 66, 2000. ISSN 361-8415. doi: http://dx.doi.org/10.1016/S1361-8415(00)00002-5. URL http://www.sciencedirect.com/science/article/pii/S1361841500000025.

[98] Z.A. Taylor, M. Cheng, and S. Ourselin. Real-time nonlinear finite element analysis for surgical simulation using graphics processing units. In *Proceedings of the 10th international conference on Medical image computing and computer-assisted intervention - Volume Part I*, MICCAI'07, pages 701–708, Berlin, Heidelberg, 2007. Springer-Verlag.

[99] Z.A. Taylor, O. Comas, M. Cheng, J. Passenger, D.J. Hawkes, D. Atkinson, and S. Ourselin. On modeling of anisotropic viscoelasticity for soft tissue simulation: Numerical solution and gpu execution. *Medical Image Analysis*, 13(2):234–244, October 2009.

[100] J. Teran, S. Blemker, V. Ng Thow Hing, and R. Fedkiw. Finite volume methods for the simulation of skeletal muscle. In *Proceedings of the 2003 ACM SIGGRAPH/Eurographics symposium on Computer animation*, SCA '03, pages 68–74, Aire-la-Ville, Switzerland, Switzerland, 2003. Eurographics Association. ISBN 1-58113-659-5. URL http://dl.acm.org/citation.cfm?id=846276.846285.

[101] J. Teran, E. Sifakis, S.S. Blemker, V. Ng-Thow-Hing, C. Lau, and R. Fedkiw. Creating and simulating skeletal muscle from the visible human data set. *Visualization and Computer Graphics, IEEE Transactions on*, 11(3):317–328, 2005. ISSN 1077-2626. doi: 10.1109/TVCG.2005.42.

[102] Demetri Terzopoulos and Kurt Fleischer. Modeling inelastic deformation: viscolelasticity, plasticity, fracture. In *Proceedings of the 15th annual conference on Computer graphics and interactive techniques*, SIGGRAPH '88, pages 269–278, New York, NY, USA, 1988. ACM. ISBN 0-89791-275-6. doi: 10.1145/54852.378522. URL http://doi.acm.org/10.1145/54852.378522.

[103] Demetri Terzopoulos, John Platt, Alan Barr, and Kurt Fleischer. Elastically deformable models. In *Proceedings of the 14th annual conference on Computer graphics and interactive techniques*, SIGGRAPH '87, pages 205–214, New York, NY, USA, 1987. ACM. ISBN 0-89791-227-6. doi: 10.1145/37401.37427. URL http://doi.acm.org/10.1145/37401.37427.

[104] D. Thalmann, Jianhua Shen, and E. Chauvineau. Fast realistic human body deformations for animation and vr applications. In *Computer Graphics International, 1996. Proceedings*, pages 166–174, 1996. doi: 10.1109/CGI.1996.511798.

[105] G. Harry van Lenthe and Ralph Müller. Prediction of failure load using micro-finite element analysis models: Toward in vivo strength assessment. *Drug Discovery Today: Technologies*, 3(2):221 – 229, 2006. ISSN 1740-6749. doi: http://dx.doi.org/10.1016/j.ddtec.2006.06.001. URL http://www.sciencedirect.com/science/article/pii/S1740674906000242.

[106] F.J. Vermolen and J.A. Adam. A finite element model for epidermal wound healing. In Yong Shi, GeertDick Albada, Jack Dongarra, and PeterM.A. Sloot, editors, *Computational Science – ICCS 2007*, volume 4487 of *Lecture Notes in Computer Science*, pages 70–77. Springer Berlin Heidelberg, 2007. ISBN 978-3-540-72583-1. doi: 10.1007/978-3-540-72584-8_10. URL http://dx.doi.org/10.1007/978-3-540-72584-8_10.

[107] F.J. Vermolen and E. Javierre. A suite of continuum models for different aspects in wound healing. In Amit Gefen, editor, *Bioengineering Research of Chronic Wounds*, volume 1 of *Studies in Mechanobiology, Tissue Engineering and Biomaterials*, pages 127–168. Springer Berlin Heidelberg, 2009. ISBN 978-3-642-00533-6. doi: 10.1007/978-3-642-00534-3_6. URL http://dx.doi.org/10.1007/978-3-642-00534-3_6.

[108] J.D. Vetter, R.G. Topazian, M.H. Goldberg, and D.G. Smith. Facial fractures occurring in a medium-sized metropolitan area: recent trends. *International Journal of Oral and Maxillofacial Surgery*, 20:214–216, 1991.

[109] Jane Wilhelms and Allen Van Gelder. Anatomically based modeling. In *Proceedings of the 24th annual conference on Computer graphics and interactive techniques*, SIGGRAPH '97, pages 173–180, New York, NY, USA, 1997. ACM Press/Addison-Wesley Publishing Co. ISBN 0-89791-896-7. doi: 10.1145/258734.258833. URL http://dx.doi.org/10.1145/258734.258833.

[110] David A. Winter. *Biomechanics and Motor Control of Human Movement*. John Wiley and Sons, Inc., Hoboken, New Jersey, third edition, 2005.

[111] IC Wright, RICHARD R Neptune, ANTON J van den Bogert, and BENNO M Nigg. The effects of ankle compliance and flexibility on ankle sprains. *Medicine and science in sports and exercise*, 32(2):260–265, 2000.

[112] I.C Wright, R.R Neptune, A.J van den Bogert, and B.M Nigg. The influence of foot positioning on ankle sprains. *Journal of Biomechanics*, 33(5):513 – 519, 2000. ISSN 0021-9290. doi: http://dx.doi.org/10.1016/S0021-9290(99)00218-3. URL http://www.sciencedirect.com/science/article/pii/S0021929099002183.

[113] Wen Wu and Pheng Ann Heng. A hybrid condensed finite element model with gpu acceleration for interactive 3d soft tissue cutting. *Computer Animation and Virtual Worlds*, 15(3-4):219–227, 2004. ISSN 1546-427X. doi: 10.1002/cav.24. URL http://dx.doi.org/10.1002/cav.24.

[114] Wen Wu and Pheng Ann Heng. An improved scheme of an interactive finite element model for 3d soft-tissue cutting and deformation. *The Visual Computer*, 21(8-10):707–716, 2005. ISSN 0178-2789. doi: 10.1007/s00371-005-0310-6. URL http://dx.doi.org/10.1007/s00371-005-0310-6.

[115] Mali Yu, Qiliang Huang, Renchao Jin, Enmin Song, Hong Liu, and Chih-Cheng Hung. A novel segmentation method for convex lesions based on dynamic programming with local intra-class variance. In *Proceedings of the 27th Annual ACM Symposium on Applied Computing*, SAC '12, pages 39–44, New York, NY, USA, 2012. ACM. ISBN 978-1-4503-0857-1. doi: 10.1145/2245276.2245286. URL http://doi.acm.org/10.1145/2245276.2245286.

[116] Can A. Yucesoy, Bart H.F.J.M. Koopman, Peter A. Huijing, and Henk J. Grootenboer. Three-dimensional finite element modeling of skeletal muscle using a two-domain approach: linked fiber-matrix mesh model. *Journal of Biomechanics*, 35(9):1253 – 1262, 2002. ISSN 0021-9290. doi: http://dx.doi.org/10.1016/S0021-9290(02)00069-6. URL http://www.sciencedirect.com/science/article/pii/S0021929002000696.

[117] Qing-hong Zhu, Yan Chen, and Arie Kaufman. Real-time biomechanically-based muscle volume deformation using fem. *Computer Graphics Forum*, 17(3):275–284, 1998. ISSN 1467-8659. doi: 10.1111/1467-8659.00274. URL http://dx.doi.org/10.1111/1467-8659.00274.

[118] Victor Brian Zordan, Bhrigu Celly, Bill Chiu, and Paul C. DiLorenzo. Breathe easy: model and control of simulated respiration for animation. In *Proceedings of the 2004 ACM SIGGRAPH/Eurographics symposium on Computer animation*, SCA '04, pages 29–37, Aire-la-Ville, Switzerland, Switzerland, 2004. Eurographics Association. ISBN 3-905673-14-2. doi: 10.1145/1028523.1028528. URL http://dx.doi.org/10.1145/1028523.1028528.